Late Holocene to Recent aragonite-cemented transgressive lag deposits in the Abu Dhabi lagoon and intertidal sabkha

YUZHU GE* [iD], CHELSEA L. PEDERSON* [iD], STEPHEN W. LOKIER† [iD], JAN P. TRAAS*, GERNOT NEHRKE‡, ROLF D. NEUSER*, KATJA E. GOETSCHL§ and ADRIAN IMMENHAUSER*

Institute for Geology, Mineralogy and Geophysics, Ruhr-Universität Bochum, Universitätsstraße 150, Bochum, 44801, Germany (E-mail: adrian.immenhauser@rub.de)
†*School of Ocean Sciences, Bangor University, Bangor, Gwynedd, LL57 2DG, UK*
‡*Alfred Wegener Institute for Polar and Marine Research, Am Handelshafen 12, Bremerhaven, 27570, Germany*
§*Institute of Applied Geosciences, Graz University of Technology, Rechbauerstrasse 12, Graz, 8010, Austria*

Associate Editor – Hairuo Qing

ABSTRACT

Modern cemented intervals (beachrock, firmgrounds to hardgrounds and concretionary layers) form in the lagoon and intertidal sabkha of Abu Dhabi. Seafloor lithification actively occurs in open, current-swept channels in low-lying areas between ooid shoals, in the intertidal zone of the middle lagoon, some centimetres beneath the inner lagoonal seafloor (i.e. within the sediment column) and at the sediment surface the intertidal sabkha. The concept of 'concretionary sub-hardgrounds', i.e. laminar cementation of sediments formed within the sediment column beneath the shallow redox boundary, is introduced and discussed. Based on calibrated radiocarbon ages, seafloor lithification commenced during the Middle to Late Holocene (*ca* 9000 cal yr BP), and proceeds to the present-day. Lithification occurs in the context of the actualistic relative sea-level rise shifting the coastline landward across the extremely low-angle carbonate ramp. The cemented intervals are interpreted as parasequence boundaries in the sense of 'marine flooding surfaces', but in most cases the sedimentary cover overlying the transgressive surface has not yet been deposited. Aragonite, (micritic) calcite and, less commonly, gypsum cements lithify the firmground/hardground intervals. Cements are described and placed into context with their depositional and marine diagenetic environments and characterized by means of scanning electron microscope petrography, cathodoluminescence microscopy and Raman spectroscopy. The morphology of aragonitic cements changes from needle-shaped forms in lithified decapod burrows of the outer lagoon ooidal shoals to complex columnar, lath and platy crystals in the inner lagoon. Precipitation experiments provide first tentative evidence for the parameters that induce changes in aragonite cement morphology. Data shown here shed light on ancient, formerly aragonite-cemented seafloors, now altered to diagenetic calcites, but also document the complexity of highly dynamic near coastal depositional environments.

Keywords Carbonate cement, early-marine cementation, Gulf, hardgrounds, seawater chemistry.

INTRODUCTION

Early diagenetic cementation of carbonate-dominated sediments at the seafloor is a common process throughout much of Earth's history (Clari *et al.*, 1995; Christ *et al.*, 2015). Lithification of sediments by various cements leads to the formation of firmgrounds and hardgrounds described for a broad range of marine environments (Kennedy & Garrison, 1975; Brett & Brookfield, 1984; Mutti & Bernoulli, 2003; De Boever *et al.*, 2017). The conventional view is that early cementation occurs at, or close to, the sediment–water interface (Kennedy & Garrison, 1975), and is typically inferred to reflect low rates or cessation of sediment deposition (Shinn, 1969; Mutti & Bernoulli, 2003; cf. 'omission surfaces', Föllmi, 2016). The majority of previous studies of marine firmground/hardground formation have dealt with ancient deposits (*ca* 750 of a total of *ca* 950 papers, Christ *et al.*, 2015), where there is significant potential for the loss of primary depositional information (Strasser, 2015). This is particularly true for hardgrounds lithifying predominantly aragonitic sediments by means of aragonitic fabrics. During subsequent burial diagenesis, these features often become diagenetically overprinted and are difficult to recognize. Although a range of hydrodynamic, chemical and biological mechanisms have been proposed as controls for firmground and hardground formation and alteration (Given & Wilkinson, 1985; Tribble, 1993), significant difficulties remain in defining which of these are the primary factors influencing the development and evolution of hardgrounds, and their associated cement fabrics and biota (Burton, 1993; Vousdoukas *et al.*, 2007).

The limited current understanding of the complex interaction of processes relevant in hardground formation and alteration calls for focused studies of actualistic *in situ* seafloor cementation where the direct observation of processes and products is possible. Despite some criticism suggesting that the Present is at best the key to the Pleistocene (Neumann & Land, 1975), sedimentologists have turned to actualistic carbonate depositional environments such as the Florida and Bahamas region, Barbados, Bermuda, the Persian (Arabian) Gulf (hereafter referred to as the 'Gulf'), the Red Sea, the Gulf of Mexico and the Mediterranean [refer to Christ *et al.* (2015) for a detailed overview of published work] to study Holocene and Pleistocene hardgrounds. However, the majority of work is predominantly descriptive, and focuses on palaeoecological aspects, or deals with isolated outcrops, particularly from intertidal and lagoon environments (Purser, 1969; Shinn, 1969; Friedman *et al.*, 1974; Hattin & Dodd, 1978; Holail & Rashed, 1992). Presently, studies working towards a mechanistic understanding of aragonitic firmground to hardground formation in Holocene (sub)tropical settings (Khalaf *et al.*, 1987; Whittle *et al.*, 1993) remain scarce. Because there is a clear bias towards observations from the deposits of calcite seas (mainly Jurassic and Cretaceous as well as Cambrian to Mississippian) in the literature (Christ *et al.*, 2015), aragonite-cemented hardgrounds are important aspects for study. The main reason for this bias is, arguably, the poor preservation potential of aragonite and high-Mg calcite fabrics in (sub)tropical carbonate hardgrounds of the Pennsylvanian to Early Jurassic aragonite seas (Stanley & Hardie, 1998).

With respect to the Gulf, the study area of this paper, Shinn (1969) recorded important observations from hardgrounds at study sites near Qatar and Bahrain (an area of 70 000 km^2), primarily from water depths of 1 to 30 m. Shinn (1969) documented submarine-cemented intervals with ^{14}C data ages between 8390 (±260) and 120 (±120) yr BP. More recently, Paul & Lokier (2017) focused on a regionally-important, diachronous hardground in the coastal sabkha of Abu Dhabi, which was formed during a forced regression between approximately 4600 cal yr BP and 1450 cal yr BP. Similarly, Taylor & Illing (1969), described cemented intervals from the Qatar Peninsula.

Motivated by the scarcity of studies focusing on the genesis of actualistic aragonite-cemented seafloors, this paper aims to: first, document a wide range of late Holocene to Recent, mainly aragonite-cemented firmgrounds to hardgrounds in the lagoon and intertidal sabkha of Abu Dhabi; second, to place these findings in the context of Late Holocene sea-level change and related hydrodynamics and proximal to distal patterns in depositional environments and cement fabrics; and third, where possible, to present tentative models explaining the observed features. Moreover, the concept of 'concretionary sub-hardgrounds' is introduced and proximal to distal patterns in aragonite cement morphology are documented here for the first time.

TERMINOLOGY

The terminology used in the literature to describe various early marine lithification features is perplexing. In the context of this paper, the following terminology is applied: firmground, incipient hardground, hardground, sub-hardground, discontinuity surface, lithocline, concretion (concretionary layer) and beachrock (see Christ *et al.*, 2015, for a detailed discussion of this terminology). Further, the descriptive label 'cemented interval' is proposed here as an umbrella term for all of these early diagenetic features. This study follows previous workers regarding the definition of early marine lithification features. For example, 'beachrock' refers to a friable to well-cemented rock that consists of a variable mixture of gravel-sized, sand-sized and silt-sized particles lithified by various carbonate minerals, which have formed along a shoreline (Vousdoukas *et al.*, 2007). Incipient minor seafloor lithification is referred to as 'firmground' (Christ *et al.*, 2015). A fully lithified seafloor qualifies as a 'hardground' when its upper surface has been bored, corroded or eroded, if encrusting or other sessile organisms are attached to the surface, or if pebbles derived from the bed occur in the overlying sediment (Bathurst, 1975). Wilkinson *et al.* (1985) also referred to lithified surfaces within a few centimetres below the sediment–water interface as hardgrounds. In practice, the difficulty lies in distinguishing between surface-formed hardgrounds (*sensu* Bathurst, 1975) subsequently buried beneath a thin sediment veneer and genuine 'sub-hardgrounds' (Molenaar & Zijlstra, 1997) formed within the shallow (10 to 20 cm) sediment column. 'Concretions' are portions of the sediment column that experience localized, often spatially-irregular lithification (Coimbra *et al.*, 2009). Where individual concretions coalesce laterally, then 'concretionary layers' form. The term 'discontinuity surface' (*sensu* Clari *et al.*, 1995) includes all lithified surfaces in stratigraphic sections that result from periods of non-sedimentation. The term 'lithocline' (*sensu* Purser, 1969) describes regionally-extensive, diachronous discontinuity surfaces.

GEOGRAPHICAL AND GEOLOGICAL SETTING

The Gulf is located to the north-east of the Arabian Peninsula and to the south-west of the Iranian Plateau, and is connected to the Indian Ocean via the narrow Strait of Hormuz (Fig. 1). This shallow (average water depth of 36 m) subtropical sea is *ca* 240 000 km² in area, with the greatest water depth (*ca* 100 m) found in the Strait of Hormuz (Sugden, 1963). Seawater salinity is higher (40 to 45‰) than in the adjacent Indian Ocean (35 to 37‰) (Purser & Evans, 1973) due to the combination of an arid climate and the restricted nature of the seaway (Kinsman, 1964). The southern coastline of the Gulf has a low-angle north-east-dipping topographic gradient and is considered as a modern analogue to ancient epeiric seas (Lokier & Fiorini, 2016). As part of the southern coastline of the Gulf, the Abu Dhabi coastal zone represents a modern low-angle carbonate ramp with numerous nearshore islands (Fig. 2). Ooid shoals accumulate seaward as sand bars and sand waves within the tidal channels between the islands, as well as tidal deltas at the seaward and lagoonward mouths of the tidal channels. The landward lagoons are dissected by small islands and suffer anthropological influence, such as dredging, construction and land reclamation (Lokier, 2013).

The Abu Dhabi climate is hot and arid, with a mean annual rainfall of 72 mm, concentrated in February and March, and a mean annual evaporation of 2.75 m (Lokier & Fiorini, 2016). Annual temperatures range from 7°C to over 50°C, with diurnal temperatures varying between 2°C and 26°C (Lokier & Fiorini, 2016; Paul & Lokier, 2017). The littoral humidity can reach 100% during summer, with a minimum average of 20.6% (Kinsman, 1964). The area is characterized by a microtidal range (1 to 2 m); however,

Fig. 1. Geographical location and bathymetry of the Gulf (modified from Sadrinasab & Kenarkohi, 2009). The red box indicates the study area.
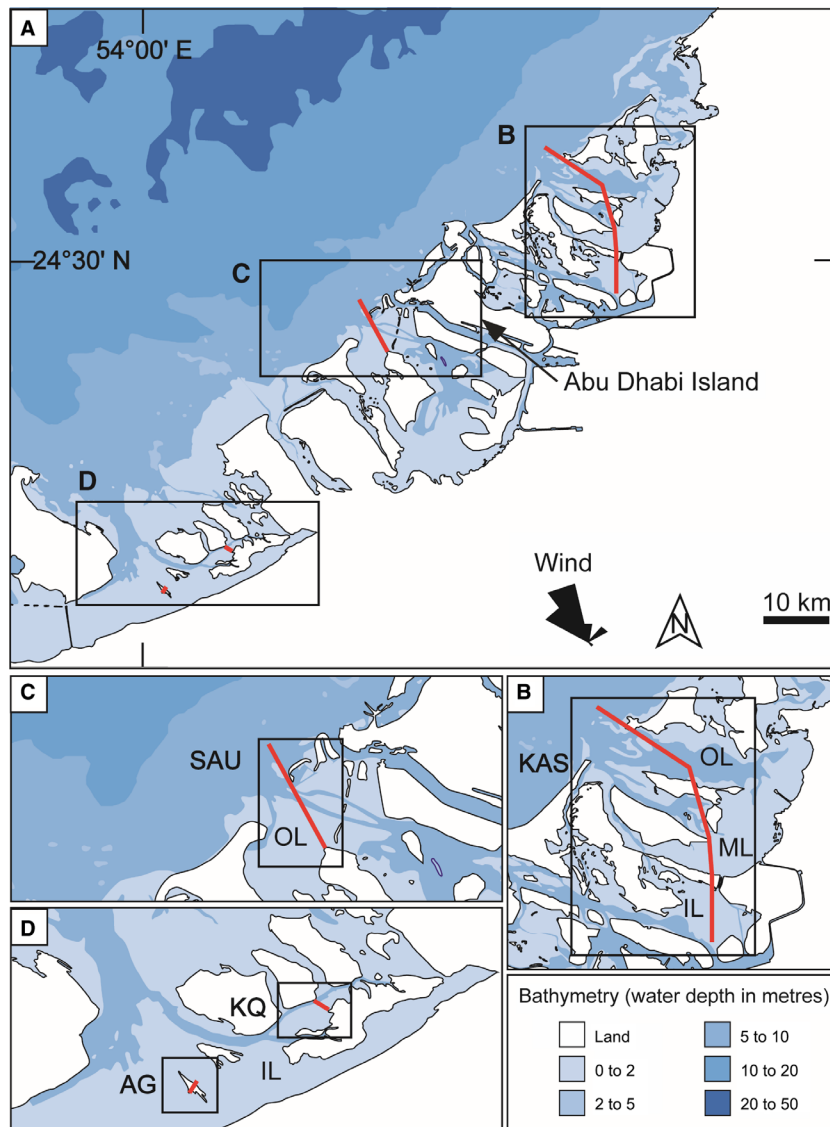
Fig. 2. Geographical location and bathymetry of the study area (sample transects are indicated by the red lines in black frames). (A) The relative location of the four studied transects along the Abu Dhabi coast. (B) The Khawr as Sadiyat (KAS) transect ranges from inner lagoon (IL), to middle (ML) and outer lagoon (OL). (C) The Shalil al Ud (SAU) transect includes outer lagoon (OL) and adjacent offshore environments. (D) The Al Gharbia (AG) and Khawr Qantur (KQ) transects both include only inner lagoon environments (IL). The bathymetry data was sourced from United Arab Emirates-Approaches to Abu Dhabi (Abu Zaby) (Marine Chart: SA_GB45050B), and the wind data from El-Sayed (1999).

strong seasonal north-north-westerly winds (Shamals) (Fig. 2) frequently produce storm surges.

The evolution of modern Abu Dhabi nearshore topography is related to eustatic changes induced by Quaternary glaciation events (Evans *et al.*, 1969; Stevens *et al.*, 2014; Lokier *et al.*, 2015). Glacioeustatic sea-level fall during the early and middle Pleistocene (>250 ka), resulted in the covering of the Abu Dhabi region by siliciclastic aeolian dunes (Ghayathi Formation; Evans *et al.*, 1969; Stevens *et al.*, 2014). Subsequent sea-level rise (*ca* 250 to 200 ka) resulted in a marine transgression and associated carbonate deposition. Renewed regression culminated in exposure and aeolian reworking of these carbonates to produce a carbonate variant of the Ghayathi Formation. A major transgressive event at *ca* 125 ka (Marine Isotope Stage – MIS – 5.5) resulted in renewed flooding of the Gulf, and deposition of the overlying Fuwayrit Formation (Stevens *et al.*, 2014). The last glaciation (*ca* 18 ka) resulted in a regional sea-level fall to *ca* 110 to 130 m lower than present day sea-level (Whitehouse & Bradley, 2013). With the termination of the glaciation, Holocene sea-level fluctuations produced a transgression from 7 to 5 ka, followed by a forced regression to present sea-level by 1440 to 1170 BP (Lokier *et al.*, 2015). More recently, the relative sea-level in the Abu Dhabi lagoon is again rising, causing a transgression with renewed flooding of the sabkha and a retrogradation of the lagoonal coastline (Lokier *et al.*, 2018). Due to the very gentle slope of the

carbonate ramp, even a small change in relative sea-level will result in a considerable lateral displacement of the coastline.

MATERIALS AND METHODOLOGY

Fieldwork and sample collection

A grid of sampling locations was defined that covered the Abu Dhabi lagoon. Sites along transects chosen for this paper were selected based on the presence of cemented intervals, accessibility and the degree of anthropogenic influence (Fig. 2). Refer to Table 1 and Figs 2 and 3 for the physiographic context of the studied transects. Three sampling campaigns (November 2017, March 2018 and January 2019) were conducted along the Abu Dhabi nearshore and adjacent offshore environments to collect sediment (hardgrounds, firmgrounds and unconsolidated sediment) and water (surface water and porewater) samples. In deeper water locations, sediment samples were collected using an Ekman grab sampler with a grab size of 15×15 cm. In the field, a hand-held Ultrameter™ (Model 6P; Myron L Company, Carlsbad, CA, USA) and refractometer were used to measure salinity, temperature, oxidation-reduction potential (ORP) and pH of water samples on site. Additional collected water samples were filtered with a 0.2 μm diameter filter into: a 2 ml plastic vial [for inductively-coupled plasma spectrometry (ICP) analysis] and a 50 ml PVC tube (for alkalinity and for repository). Air bubbles were carefully expulsed from the water samples during sampling to reduce any exchange of gases. Porewater samples were collected by inserting Rhizons (pore size of 0.12 to 0.18 μm) into the sediment profile (centimetres to some decimetres), and then transferred to their respective vials using 0.2 μm filters. In the field, all samples were kept cool to reduce microbial activity and subsequently stored in a refrigerator prior to shipping to the Ruhr-University Bochum, Germany for processing.

Optical, cathodoluminescence and scanning electron microscope analyses

Thin section and scanning electron microscopy (SEM) were performed for the cemented and unconsolidated sediments to observe fabrics and mineral compositions at Ruhr-University Bochum. The thin sections were dyed with Alizarin Red S and potassium ferricyanide (Friedman, 1959; Dickson, 1965) to distinguish carbonate mineralogy and porosity. Photographs were taken using a Zeiss optical microscope (Zeiss, Oberkochen, Germany). Freshly broken samples were washed with deionized water and coated with gold prior to SEM observation (Zeiss-Gemini 2-Merlin HR-FESEM). The SEM parameters included an acceleration voltage from 0.2 to 30 kV, a resolution of 0.8 nm at 15 kV and 1.4 nm at 1 kV. In conjunction with SEM, energy dispersive spectroscopy (EDS) was conducted for element analysis of different cement phases, specifically to separate aragonite (Mg below detection limit), calcite (*ca* 2 wt.% Mg) and gypsum cements. The cathodoluminescence microscopy facility at Ruhr-University Bochum offers access to a 'hot cathode' microscope (type HC1-LM; lumic, Dortmund, Germany). The acceleration voltage of the electron beam is 14 kV and the beam current is set to a level to produce a current density of *ca* 9 mA mm^{-2} on the sample surface.

### Geochemical analyses of water and sediment samples

Water samples were measured for alkalinity and elements at Ruhr-University Bochum. For alkalinity analysis, three drops of indicator solution (HCl) were added to a 5 ml sample. Following mixing, the solution was titrated with titration solution (HCl). Alkalinity was then calculated based on the volume of titration solution needed to produce the colour change of the solution (from blue to red). Elemental concentrations (Mg, Ca, Sr, Fe and Mn) of water samples, were measured on an inductively-coupled plasma – optical emission spectrometer (ICP–OES; Thermo iCAP 6000 Series; Thermo Fisher Scientific, Waltham, MA, USA) by mixing 1 ml sample water with 1 ml milli-Q water and 1 ml 3 M HNO$_3$. BCS-CRM 512 and 513 (dolomite and calcite) were used as standards.

Microprobe analysis was conducted using a Cameca SX Five FE (Cameca, Gennevilliers Cedex, France) equipped with five different spectrometers at the Ruhr-University Bochum. Accelerating voltage was 15 kV and beam current 20 nA. Elemental maps were created for the following elements: aluminium (Al), calcium (Ca), magnesium (Mg), sodium (Na), silica (Si) and strontium (Sr).

Table 1. Studied transects along the Abu Dhabi coastal area.

Transect	Start point	End point	Environments studied
Al Gharbia (AG)	24°8.488′N, 54°0.932′E	24°8.664′N, 54°1.203′E	Intertidal sabkha and inner lagoon
Khawr Qantur (KQ)	24°9.723′N, 54°8.000′E	24°10.992′N, 54°6.171′E	Intertidal sabkha and inner lagoon
Shalil al Ud (SAU)	24°23.575′N, 54°17.325′E	24°27.412′N, 54°14.429′E	Outer lagoon and adjacent offshore area
Khawr as Sadiyat (KAS)	24°27.607′N, 54°34.154′E	24°37.985′N, 54°28.334′E	Inner, middle, outer lagoon and adjacent offshore area
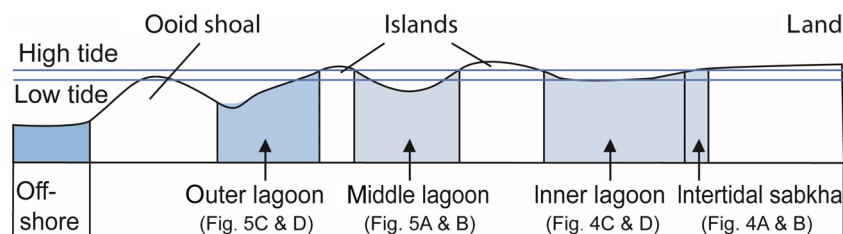
Fig. 3. Schematic cross-section of the Abu Dhabi nearshore area. Further details of each subzone are shown in the indicated figures. (Note: The horizontal direction is without scale; colours indicate water depth as referenced in Fig. 1.)

Radiocarbon dating

Four cemented samples (two from the inner lagoon and two from the outer lagoon) from the Khawr as Sadiyat transect were ^{14}C-radiocarbon dated. Between 14 mg and 100 mg of material was drilled from filter-feeding *Brachidontes* bivalve shells cemented within the hardground. Shells were examined to rule out taphonomic processes that would bias radiocarbon analysis. The drilled powders were analysed using accelerator mass spectroscopy (AMS) by Beta Analytic, Radiocarbon Dating Laboratory in London, UK. The conventional radiocarbon ages were calibrated against a marine calibration curve utilizing the CALIB calibration program (Stuiver & Reimer, 1993) applying a regional reservoir age correction of 180 ± 53 (Hughen *et al.*, 2004).

Raman spectroscopy

Raman spectroscopy was performed using a WITec alpha 300 R (WITec GmbH, Ulm, Germany) confocal Raman microscope (CRM) with a Zeiss LD Plan NEOFLUAR 20× lens at the Helmholtz Center for Polar and Marine Research at the Alfred Wegner Institute (additional reading: Nehrke & Nouet, 2011; Nehrke *et al.*, 2012; Wall & Nehrke, 2012). This method provides a quantitative characterization of carbonate mineralogies. Scans of a hardground thin section from the Khawr as Sadiyat transect were imaged using a motorized scan table. A total scan area of $700 \times 650\ \mu m$ was measured, with a resolution of $2\ \mu m$ (resulting in a total of 113 750 single Raman spectra) and an integration time of 0.1 s per Raman spectra. Excitation wavelength was 488 nm and the spectrometer an ultra-high throughput spectrometer (UHTS 300; WITec, Germany; grating 600/mm, 500 nm blaze) equipped with an electron multiplying CCD (EMCCD) camera. Data analysis was performed using the WITec Project FOUR 4.0 software.

Aragonite cement precipitation experiments

Inorganic $CaCO_3$ precipitation experiments were conducted at Graz University of Technology (Austria) in order to assess the significance of solution chemistry on mineral morphology and surface structure during aragonite growth. The detailed description of the experimental set-up has been reported by Goetschl *et al.* (2019). Briefly, the precipitation of aragonite at ambient temperature was induced by the addition of two inlet solutions in a mixed-flow reactor containing $CaCO_3$ seed material. The two inlet solutions

contained (Ca, Mg)Cl$_2$ and Na$_2$(CO$_3$, SO$_4$), respectively, and were pumped via a peristaltic pump in the reactor at a constant flow rate of *ca* 10 ml day^{-1}. The initial 0·5 L solution in the reactor contained 10 mM both CaCl$_2$ and MgCl$_2$, as well as varying concentrations of Na$_2$SO$_4$. Ionic strength of all solutions remained constant at 400 mM during each experimental run by adding NaCl if necessary. The pH was kept constant at 6·3 ± 0·1 by continuous bubbling of CO$_2$ gas into the reactive solution. An aliquot of the reactive solution was collected every 24 h with a syringe for chemical analyses, so that the volume of the reactor solution remained near constant (within ±4%). Directly after sampling, the collected solution was filtered through using a 0.2 μm membrane cellulose acetate syringe filter and the pH was measured with a calibrated pH electrode coupled to a meter using a three-point calibration. After a total experimental duration of 12 days, the solid material was collected using a suction filtration unit, rinsed with ultrapure deionized water, and dried.

RESULTS

Depositional environments and facies distribution

Based on the degree of isolation from the Gulf due to the presence of shoals and barrier islands, the nearshore area described here is broadly subdivided into four physiographic settings (Fig. 3). The terminology applied (outer, middle and inner lagoon, and intertidal sabkha) is, at best, a very coarse approximation, as water depth, level of restriction and hydrodynamics change both perpendicular and parallel to the coastline, resulting in a complex, highly dynamic system. The intertidal sabkha is studied at Al Gharbia (AG) and Khawr Qantur (KQ), the inner lagoon at Al Gharbia, Khawr Qantur and Khawr as Sadiyat (KAS), the middle lagoon at Khawr as Sadiyat and the outer lagoon at Khawr as Sadiyat and Shalil al Ud (SAU; Table 1). Please refer to Tables 2 and 3 and Figs 4 to 10 for an overview of depositional environments, bathymetry, characteristic features, sediment composition, hydrodynamic level and a systematic overview of the sedimentary and morphological characteristics of different types of cemented intervals described herein. Moreover, samples were collected from man-made exposures of Pleistocene cemented

intervals resulting from channel-building projects. These are located a few kilometres southeast of the southern extension of the KQ transect.

Macroscopic and sedimentological properties of cemented intervals

Intertidal sabkha
Firmgrounds at the surface of the intertidal sabkha at KQ occur as lithified carbonate units with a black-stained, irregular, mammillated upper surface microtopography (Table 3; Fig. 7A). These firmgrounds are laterally discontinuous, often as isolated patches (predominantly 0.4 to 1.0 m in size) separated by pervasively-bioturbated unconsolidated sediment. The lower surfaces of these firmgrounds are irregular and display numerous hollows 1 to 5 cm in diameter (Fig. 7A). The amount of cementation decreases downward within the firmground, passing into completely unlithified sediment at a depth of 3 to 6 cm. No boring or biotic encrustation is observed. Landward, at AG (Fig. 2D), these firmgrounds are broken up and reworked to produce clasts some centimetres to some decimetres in diameter (Fig. 6A). The firmgrounds are locally covered by a thin sediment veneer washed onto the cemented intervals by wave and current activity.

Inner and middle lagoon
In the inner and middle lagoon, seafloor lithification is widespread and variable (Table 3). Fully-lithified hardgrounds are exposed at the seafloor, and locally covered by coarse bioclastic sediment, (pel)ooidal sands, or carbonate silt and mud. Locally-developed thin, friable crusts are covered by some tens of centimetres of carbonate mud, silt and sand. In the inner lagoon of KQ (Fig. 2D), bordering the intertidal sabkha, three distinct hardground layers (top layer, 1.0 to 1.5 cm thick; middle layer, 1 to 2 cm; bottom layer, 1 to 3 cm) are vertically separated by unconsolidated sediment (2 to 4 cm; Fig. 6B). These 'stacked' hardgrounds exhibit a down-section increase in cementation and a change in colour from white to grey. The top hardground is either exposed or locally covered by *ca* 2 cm of sediment. The upper surfaces of the hardgrounds are flat with rare borings (<1 to 3 mm), and the lower surfaces are irregular.

At the high energy setting of AG (Fig. 2D), the cemented intervals are exposed at the seafloor (Fig. 4C) or locally covered by about 10 to 50 cm unconsolidated sediment (generally

Table 2. Depositional environments and facies distribution. Refer to Figs 2 and 3 for key to transects, and Figs 4 to 6 for more details.

Physiography	Bathymetry	Main features	Sediment composition	Hydrodynamic energy
Intertidal sabkha	0–0.5 m 0.2–0.4 m in tidal creeks	Microbial mats with large polygon structure (up to 1 m in diameter)	KQ: peloids (60–80%), with silt and clay (20–40%). AG: sand-grade grains (80–90%) consisting of peloids (40–80%), gastropods (6–40%), foraminifera (3–15%) and quartz grains (0–9%)	Very low level along the KQ transect. Locally higher energy (due to the lack of barrier islands) along the AG transect
Inner lagoon	Exposed at low tide, <2 m at high tide	Wave and current ripples are abundant in areas devoid of seagrass. In the middle portions of the KAS transect, a network of centimetres-deep to a few decimetres-deep tidal channels and lobate erosional scours are found	Sediment dominated by peloids (30–90%), gastropods (1–30%), foraminifera (1–20%), bivalves (1–16%) and quartz grains (1–15%). Narrow nearshore belt is made up of well-sorted carbonate sands. Skeletal and quartz grains (<14%) are abundant in inner AG lagoon. Peloids and aggregate grains (3–8%) are abundant at KQ and KAS	Low, when protected by barrier islands to moderately high under the influence of high, north-north-westerly winds (Shamals). Wave-base and seafloor interaction can stir up sediment
Middle lagoon	Locally exposed at low tide, <3 m at high tide	Middle lagoon lies within the inner island complex between the former two environments. Locally, the barren seafloor is composed of hardgrounds in part covered by thin veneer of shell debris. Large polygonal systems of cracks (mega-polygons) are exposed during low tide	KAS: Unconsolidated sediment is colonized by mangroves and seagrass. Seaward, peloids (50%), gastropods (20%) and foraminifera (15%) dominate sediment (bioclasts <5 cm in diameter to mud grade). Arenitic carbonate increases in abundance (60–70%) landward. Quartz grains (2–3%) component, with carbonate mud (1–6%) and silt (14–43%) fractions increase landward	Low, when protected by barrier islands to high in open settings and under the influence of high, north-north-westerly winds (Shamals). Wave-base and seafloor interaction can stir up and winnow sediment
Outer lagoon and offshore	Locally exposed (ooid shoals) to <10 m in tidal channels	In comparison to the lagoonal environments, which are influenced by tidal interactions between the small islands, the offshore area represents open-water conditions dominated by wave and current action. In the broad tidal channels, the seafloor may be swept clean or locally covered by migrating sand dunes	At KAS and SAU, tidal channels with ooid shoal complexes that terminate landward and seaward. Inter-shoal areas are characterized by seagrass with epiphytic bivalves, gastropods and foraminifera. Ooids (60–90%), gastropods (4–40%) and calcareous algae (2–40%) are main composition. Grain size is variable, with clay and silt components reaching up to 36% in inter-shoal areas covered by seagrass, and up to 88% coarse sand on shoals	Low on days of low wind strengths but dominated by intense tidal currents. High during high wind events. Strong wave base and current interaction at ooidal shoals

Table 3. Sedimentary and morphological characteristics of different types of cemented intervals.

Type	Location	Environment	Water depth (m)	Sediment cover (cm)	Thickness (cm)	Upper surface	Lower surface	Evidence of encrustation	Cement fabric morphology and mineralogy
Actualistic firmground	Khawr Qantur	Intertidal, low energy	0.0–0.3	0–1	3–6	Irregular	Irregular with hollows	None	Lath, platy, columnar and prismatic aragonite. Some round voids at terminations of prismatic aragonite. High-Mg calcite micrite
Concretionary (sub) hardground	Khawr as Sadiyat	Inner lagoon, low energy	0.0–1.0	15–20	8–20	Planar	Irregular	None	Lath, platy, columnar and prismatic aragonite. Common round voids at terminations of prismatic aragonite. High-Mg calcite micrite
Inner-lagoon hardground grading into beachrock	Al Gharbia	Inner lagoon, high energy	0.0–0.6	0–50	12–20 to <1 landward	Planar	Irregular	Only common on the lower surface	Lath, platy, columnar, prismatic, fibrous and acicular aragonite. Rare round voids at terminations of prismatic aragonite. High-Mg calcite micrite
Lagoon hardground with eroded tepees	Khawr as Sadiyat	Middle to outer lagoon, medium energy	0.5–2.0	0–2	5–15	Planar	Irregular	None	Lath, platy, columnar, prismatic, fibrous and acicular aragonite. Common round voids at terminations of prismatic aragonite. High-Mg calcite micrite. Polygonal gypsum
Lithified decapod burrows	Khawr as Sadiyat	Outer lagoon, high energy	1.0–5.0	>5	3–15	Irregular	Irregular	Common on all surfaces	Acicular aragonite

Fig. 4. Field images from the intertidal sabkha and inner lagoon. (A) Intertidal sabkha microbial mats at Khawr Qantur (KQ) showing well-developed polygon structures. (B) Seaward edge of the microbial mats at the KQ intertidal sabkha, showing patchy distribution (black arrow) separated by unconsolidated sediment. (C) Lithified fractured hardground of the Al Gharbia (AG) inner lagoon covered by shallow water. (D) An exposed shoal from the Khawr as Sadiyat (KAS) inner lagoon, with localized algae (black arrow) growing on bioclasts. Image taken at low tide.
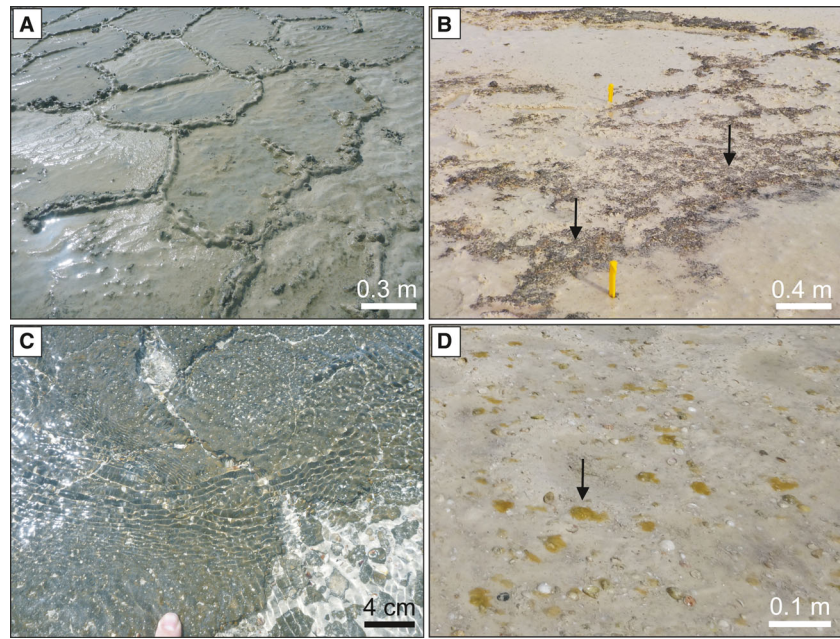
seaward; Fig. 7B). The black upper surfaces of the hardgrounds are flat with protruding skeletal fragments, and the lower surfaces are irregular. These hardgrounds are up to 20 cm thick, but display a downsection and landward decrease of cementation, qualifying as firmgrounds at best (Figs 6A and 8E). Borings are not common, and encrustation by bivalves is ubiquitous on lower surfaces of exposed portions of the hardground (Fig. 8C).

In the middle to inner KAS lagoon (Fig. 2B), hardgrounds also range in thickness, continuity and degree of cementation. Fully-lithified successions up to 50 cm thick, of variably cemented sediment (Fig. 9C) occur near dredged channels at water depths of 1 to 2 m (Table 3; Fig. 9). Hardgrounds of a few centimetres in thickness, brittle firmgrounds covered by 2 to 50 cm of unconsolidated sediment and marine plants occur in the most proximal settings. Both exposed and sediment-covered hardgrounds show conspicuously flat upper surfaces and a downward decrease in cementation. Where areas of the seafloor are locally denuded and exposed, centimetre-wide fissures form metre-sized polygons in the hardground (Fig. 9). The fissures are commonly filled by coarse bioclastic material and other sand-sized carbonates (Fig. 9D).
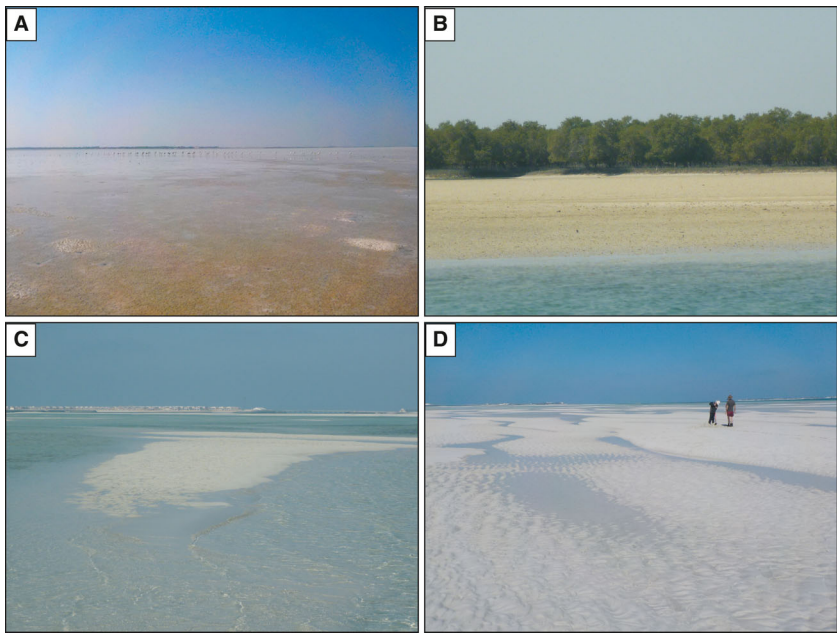
Outer lagoon

Two types of lithification are present in the outer KAS lagoon (Table 3). Fully-lithified hardgrounds form on the seafloor in high-energy

tidal channels at water depths of about 10 m and sand waves migrate across the otherwise barren seafloor. These features are not described in detail here as the evidence is indirect, originating from grab sampling. Here, the focus is on intershoal areas, where the seafloor is patchily covered by seagrass (Figs 6D and 10) and cemented intervals are either exposed or covered by a thin and constantly moving sediment veneer (Fig 10). Hardground intervals occur as cemented decapod burrow networks and irregular to patchy tabular nodules (some tens of centimetres in diameter); perhaps representing an amalgamation of several closely-spaced burrows (Fig. 10). In many locations, up to *ca* 80% of the sediment consists of the friable to hard carbonate burrows. Individual cemented burrows have a very irregular morphology, typically some centimetres in diameter and extend over many tens of centimetres (Fig. 10). Rare bivalves and barnacles encrust the upper surface of the hardground, while serpulid encrustation is ubiquitous.

Cemented intervals: radiocarbon ages, mineralogy and cement fabrics

An overview of previously published radiocarbon ages and new data obtained in the context of this study are shown in Fig. 11. Here, *Brachidontes* bivalve shell fragments (avoiding endolithic shells) encased in the cemented intervals from the inner KAS lagoon yield ^{14}C ages

Fig. 5. Field photographs from the middle and outer lagoon. (A) Extremely shallow water with localized exposure at the Khawr as Sadiyat (KAS) middle lagoon during low tide. The width of the image in the foreground is *ca* 5 m. (B) Localized mangroves in the KAS middle lagoon. The mangroves are *ca* 3 m high. (C) Exposed ooid shoal during low tide at the KAS outer lagoon. The width of the image in the foreground is *ca* 6 m. (D) Wave ripples and tidal creeks on the crest of a Shalil al Ud (SAU) outer lagoon ooid shoal (persons to the right are *ca* 1.8 m tall).

Fig. 6. Seafloor features from the intertidal to outer lagoon. (A) Firmgrounds break into centimetre to decimetre scale intraclasts (tape measure for scale is *ca* 20 cm in length) in the Al Gharbia (AG) intertidal zone. (B) Lithified interval from the Khawr Qantur (KQ) inner lagoon. Thin sediment cover has been removed by hand. (C) Abundant bioclasts and unconsolidated sediment in the Khawr as Sadiyat (KAS) middle lagoon (hammer head is *ca* 15 cm in length for scale). (D) Seagrass with unconsolidated ooids and bioclasts from the KAS outer lagoon. Note the strong current originating from left of image.
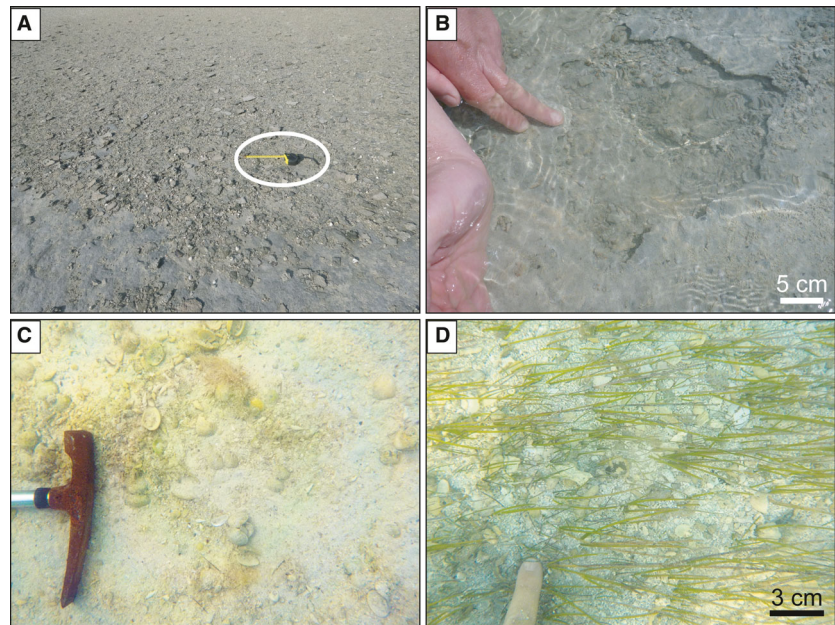
between 268 cal yr BP and 0 cal yr BP. This Recent age for the bivalves proves actualistic hardground formation within the inner lagoon. Radiocarbon ages of 628 to 422 cal yr BP and 608 to 358 cal yr BP are determined from bivalves in cemented intervals of the outer lagoon ooid shoal belt.

The cemented intervals (Table 3) contain aragonite cements (Figs 12 and 13) with a wide spectrum of morphologies and locally abundant micritic (calcitic; Figs 12A and 13) and gypsum cements (Fig. 12B). Elemental analyses (EDS and microprobe), and particularly mineralogy data (Raman spectroscopy; Fig. 14) and crystal morphologies, collectively conclude acicular, fibrous, elongate prismatic, lath and platy cements to be aragonitic, and marine in origin (Fig. 12). High-Mg calcite cements display orange, while aragonite cements are characterized by dark red to purple luminescence (Fig. 13).
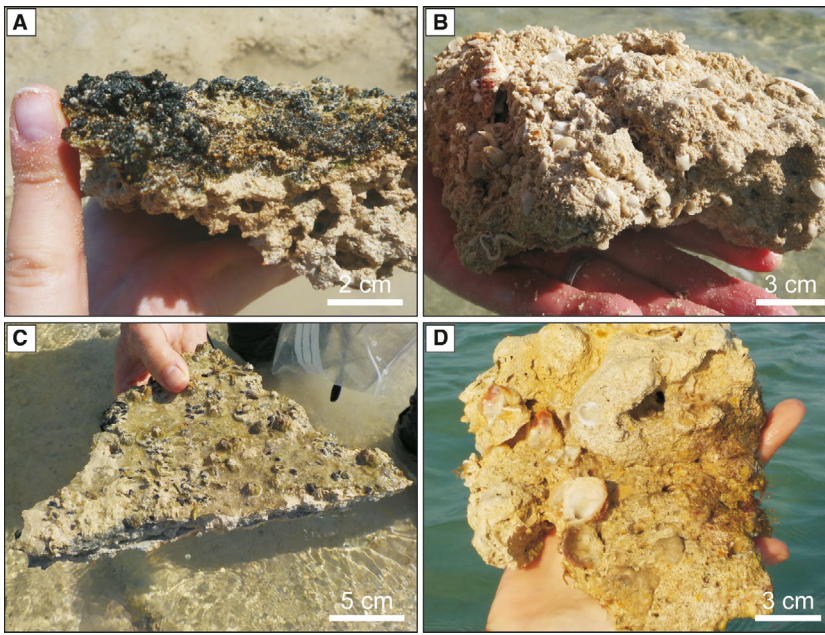
Fig. 7. Macroscopic variation of cemented intervals. (A) Khawr Qantur (KQ) intertidal sabkha firmground with irregular surface, consisting of microbial cover and underlying lithified sediment with vuggy porosity. (B) Al Gharbia (AG) inner lagoon hardground with irregular lower surface. Components include coarse bioclastic sediment. (C) Near-planar lithified interval encrusted by algae and molluscs from the Khawr as Sadiyat (KAS) inner lagoon. (D) Outer KAS lagoon hardground with irregular and nodular surfaces, containing bivalve encrustation and borings.

Acicular cements present as needle crystals (Sandberg, 1985) dominate the cemented intervals in the outer lagoon adjacent to the offshore environment (Table 3; Fig. 12D). Acicular cements with pointed terminations are oriented perpendicular to grain surfaces and occur as isopachous fringes around bioclasts, peloids or ooids (Figs 12 and 15). In order to avoid confusion, crystal dimensions (or ranges thereof) will be presented in terms of length (L): width (W): thickness (T) ratios. L:W:T ratios of acicular cements are 10–40:1–2:1–2 μm.

Morphologically, fibrous cements (Fig. 12E) are among the dominant fabrics in the cemented intervals of the outer and (partially) middle lagoon. Fibrous cements have flattened rather than pointed terminations and grade into crystals that are columnar in shape. The orientation of the fibrous cements is perpendicular and in places random relative to grain surfaces, particularly where the surface morphology is very irregular due to microendolithic borings (Fig. 12E and F). Fibrous crystals have L:W:T ratios of 10–20:1:1 μm.

Elongate prismatic (pseudo-hexagonal) cements show intergrowth with lath and platy cements in the intertidal sabkha and inner lagoon (Fig. 12G). The elongate prismatic cements have flattened terminations and well-defined crystal surfaces. The cements project outward from grain surfaces at random orientations. Elongate prismatic crystals have L:W:T ratios of 10–25:5–12:2–3 μm. Round voids frequently occur at the outward crystal terminations (Fig. 12G). Elongate prismatic, lath and platy cements are often associated with numerous framboids reaching 10 μm in diameter (Fig. 12H).

Cemented intervals in the intertidal sabkha and inner lagoon contain aragonite with a complex morphological succession, with fabrics ranging from needle-like to fibrous cements that grade into arrays of bifurcating fibrous cements, lath-cements and, finally, platy morphotypes (Figs 12 and 15). These cements project outward from grain surfaces at random angles (Fig. 15C and D). In the inner KQ and KAS lagoons, the L:W:T ratios are 4–10:3–6:2–4 μm in width. In the AG inner lagoon, L:W:T ratios are 2–8:1–2:1–2 μm.

Microcrystalline and micritic cements (Marshall & Davies, 1981) occur as micron-sized (1 to 4 μm long), often curved-rhombic high-Mg calcite crystals with about 2 wt.% Mg (Figs 12A and 13). This common form of submarine cement is likely generated by direct chemical precipitation and should not be confused with detrital micrite, which may result from the disaggregation of carbonates and other processes, such as the formation of destructive micritic envelopes. In some cases, micritic cements form the substratum of the above-mentioned acicular cements. These cements either coat grain surfaces as thin rims or accumulate as micro-peloids. Often, micritic cements overgrow calcitic substrata (for example, calcitic foraminifera tests; Fig. 12A), as well as aragonitic gastropods (Fig. 13). This cement
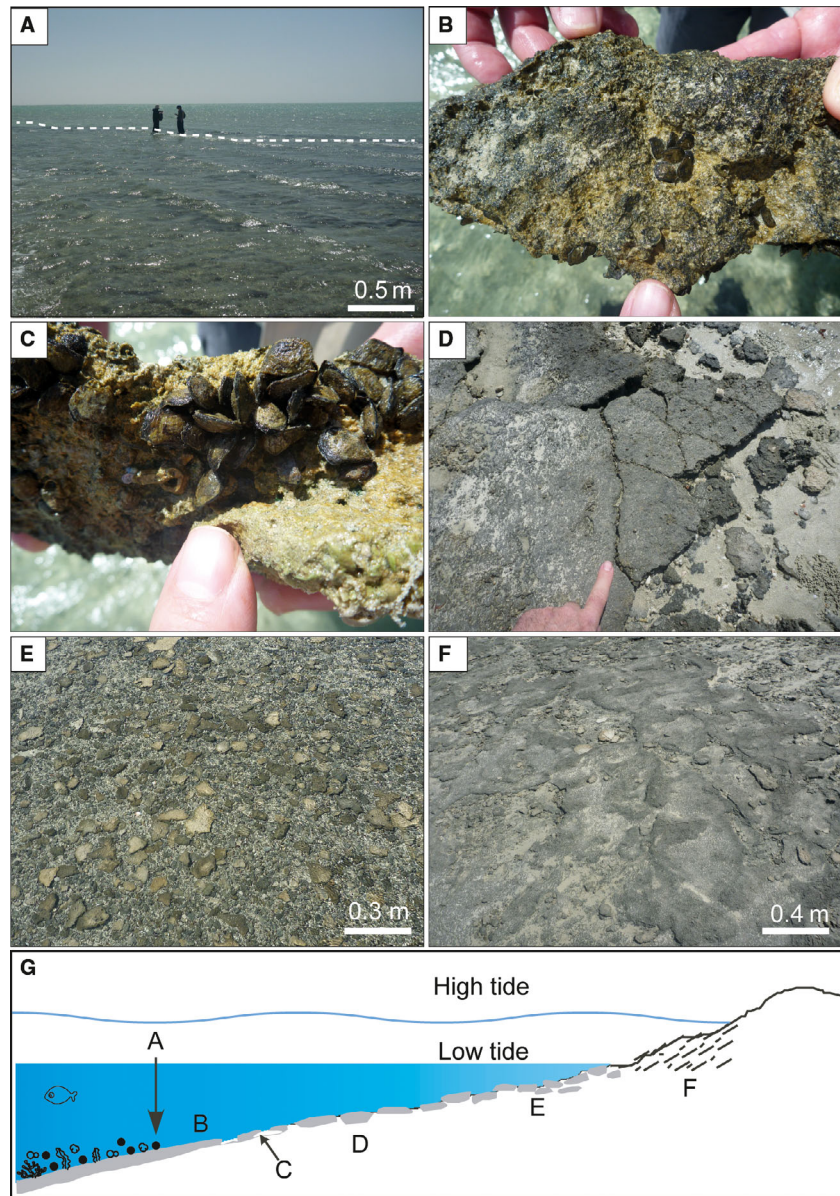
Fig. 8. Spatial variation of cemented intervals along the Al Gharbia (AG) transect. (A) The boundary (white stippled line) between the relatively shallow lithified seafloor and the deeper uncemented seafloor (persons of about 1.7 m height for scale). (B) The upper surface of shallower-water cemented intervals encrusted by biofilm and rare bivalves. (C) The lower surface of cemented intervals – landward but similar to (B) encrusted by abundant bivalves. (D) The initial break-up of cemented intervals from (B) and (C). (E) Continued break-up of hardground intervals, resulting in centimetre to decimetre scale intraclasts near beach. (F) Intertidal, centimetre-thin, leather-like beachrock. (G) A schematic figure of the cemented intervals along the transect with corresponding location of (A) to (F).

phase is very abundant, but the abundances show significant lateral variability over distances of some metres only, in some hardground samples in the middle lagoon. In places, micritic cements may form up to 50% of the hardground cement phase (Fig. 13). Authigenic gypsum crystals are present as stubby to elongate prismatic cements in well-developed hardgrounds of the middle lagoon (Fig. 12B).

Spatial trends in seawater and porewater properties

Seawater and porewater properties were obtained during the first two field periods.

Between the two periods, seawater properties are relatively consistent in salinity and pH. In contrast temperature, oxidation-reduction potential (ORP), alkalinity and elemental concentrations are all variable between November 2017 and February to March 2018 (Fig. 16). Comparisons between seawater and shallow, oxidized porewater samples suggest that alkalinity and elemental concentrations of both fluid types are indistinguishable within error (Fig. 16). Salinity values show a decreasing trend seaward. Generally, the most significant difference of salinity is between the intertidal sabkha and inner lagoon, whereas salinity remains relatively stable from the inner lagoon to offshore areas. Temperature
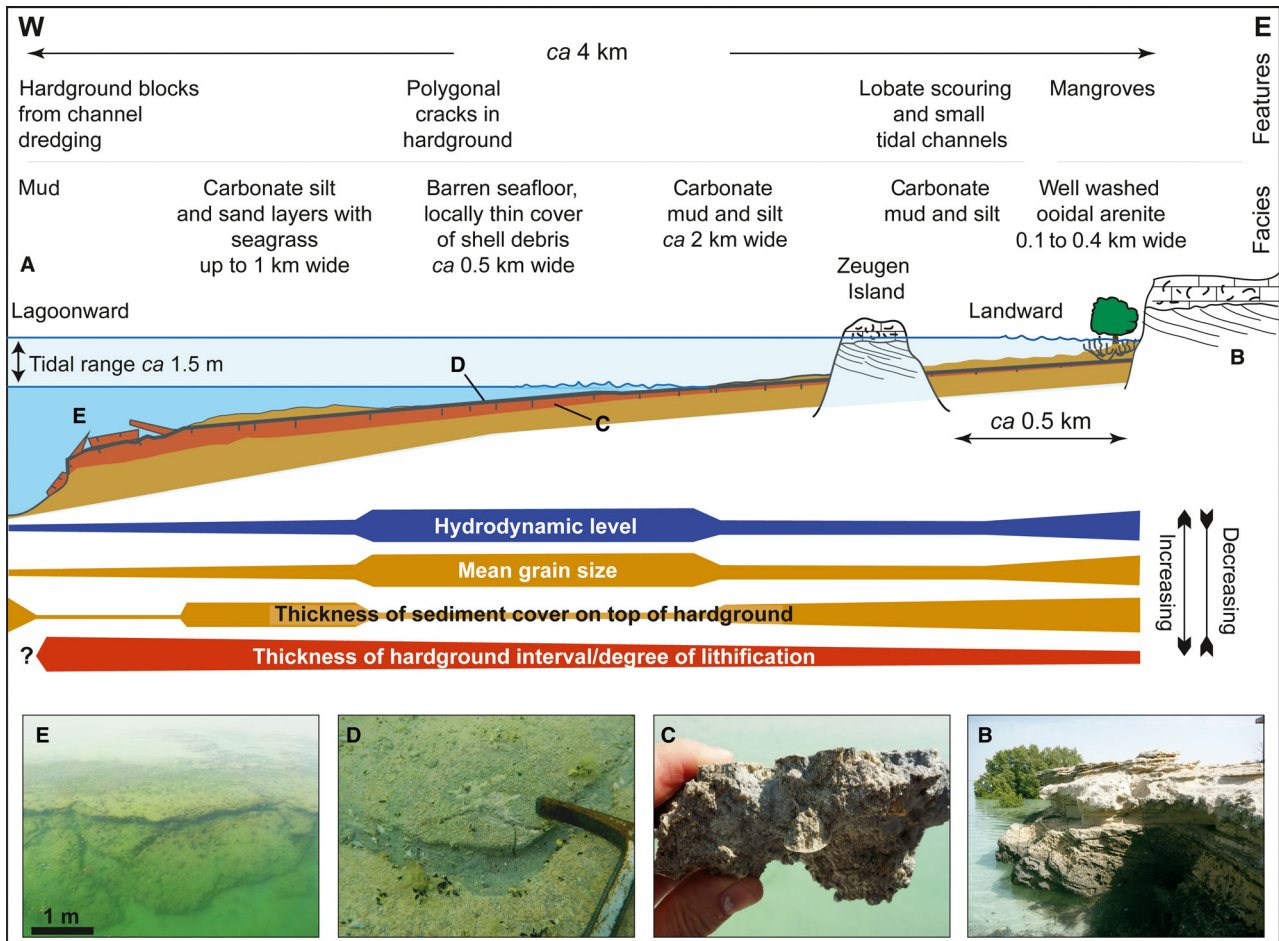
Fig. 9. Schematic of a landward to seaward profile of the development of hardgrounds, with the associated environmental factors in the Khawr as Sadiyat (KAS) middle to outer lagoon. (A) Illustration of landward–seaward changes in seafloor composition, hardground development, hydrodynamic level and mean grain size. (B) Outcrop of Pleistocene sedimentary rocks at shoreline. (C) Hardground from the submarine polygonal cracks. (D) Polygonal cracks in submarine hardgrounds filled with unconsolidated sediment. (E) The exposure of several stacked and amalgamated hardground intervals reaching 50 cm in thickness along the edge of a dredged channel.

data show a similar trend but fluctuate between different times of the year. Higher seawater temperatures were recorded in November 2017 (average = *ca* 28°C, *n* = 4) compared to March 2018 (average = 24 to 25°C, *n* = 24). Alkalinity decreases from 2.2 to 1.6 mmol l^{-1} within the intertidal sabkha and shows differences between the field periods (average = 2.72 mmol l^{-1}, *n* = 5, November 2017; average = 2.13 mmol l^{-1}, *n* = 27, March 2018) (Fig. 16).

No obvious differences of Mg/Ca molar ratios between seawater and shallow porewater samples are observed but more detailed work and, specifically, monitoring are required. These ratios show higher values in November 2017. Magnesium/calcium molar ratios, furthermore,

vary between environments, with the lowest values in the inner lagoon (4.6 to 5.3), mid-range values in the outer lagoon to offshore area (4.8 to 5.3) and the highest values in the intertidal sabkha environment (>5.0; Fig. 16).

Aragonite precipitation experiments

X-ray diffraction (XRD) patterns of laboratory carbonate precipitates performed in the context of the study by Goetschl *et al.* (2019) are indicative for calcite and aragonite. The highest proportions of aragonite were precipitated in experiments conducted at fast mineral growth rates (growth rate > $10^{-7.2}$ mol m^{-2} s^{-1}) and 30 mM sulphate concentration (similar to
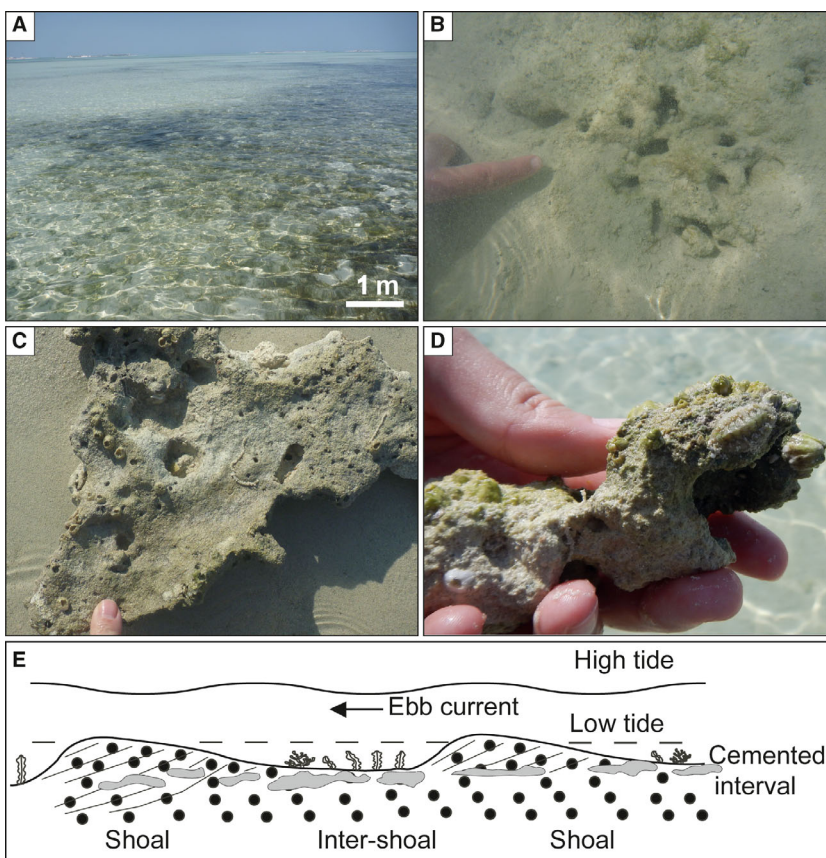
Fig. 10. Cemented intervals from the ooid shoal environment. (A) Shallow water depth and seagrass colonization (dark areas). The width of the image in the foreground is *ca* 7 m. (B) Subaqueous concretionary cemented decapod burrow network interval. Note the holes formed due to unconsolidated sediment removed by currents. (C) The upper surface of an encrusted, ooid shoal-associated cemented interval. (D) The typical irregular morphology of a lithified decapod burrow. (E) Schematic of hardground occurrence in the ooid shoal setting. Grey colour refers to cemented burrow network.

seawater concentration) prevailing in the reactive solution. The SEM photographs of precipitates collected at the end of the experiments show elongated aragonite prisms with a pseudo-hexagonal shape. The observed porous surface structure of the (001) aragonite crystal surface resulted from experiments performed with Mg^{2+} and SO_2^{4-} bearing solutions.

INTERPRETATIONS AND DISCUSSION

Holocene sea-level change in the Gulf

Holocene sea-level rise led to rapid flooding of the Gulf sedimentary basin (Fig. 11) and the onset of widespread hardground formation throughout the open Gulf (average water depths of 35 m). Transgression reached the position of the current shoreline, and the position of the study area, by the Middle Holocene, briefly peaking *ca* 1 m above present day sea-level at *ca* 4570 cal yr BP, before declining below current levels by 1440 to 1170 cal yr BP (Lokier *et al.*, 2015) (Fig. 11). Radiocarbon ages indicate that

the lithification features described herein post-date the late Holocene regression (Fig. 11) and must be placed in the context of the more recent sea-level rise, leading to renewed flooding of the tectonically-stable, southern shore of the Gulf. Five characteristic case examples of seafloor and sub-seafloor lithification are described, interpreted and placed in the context of published work (see Table 3 for a systematic overview of the different types of cemented intervals).

Cemented intervals

The extremely low gradient (0.07 to 0.08°) of the Abu Dhabi carbonate ramp system results in significant seaward–landward displacement of the coastline and of facies belts even with small changes in sea-level. This is exemplified in the significant shifts (>2 km) of the waterline across a single tidal cycle (mean amplitude of *ca* 1.5 m). On the basis of field observations and radiocarbon dating of cemented intervals, the cementation features described here are geologically very young and processes are active to the present day. The zone of active lithification
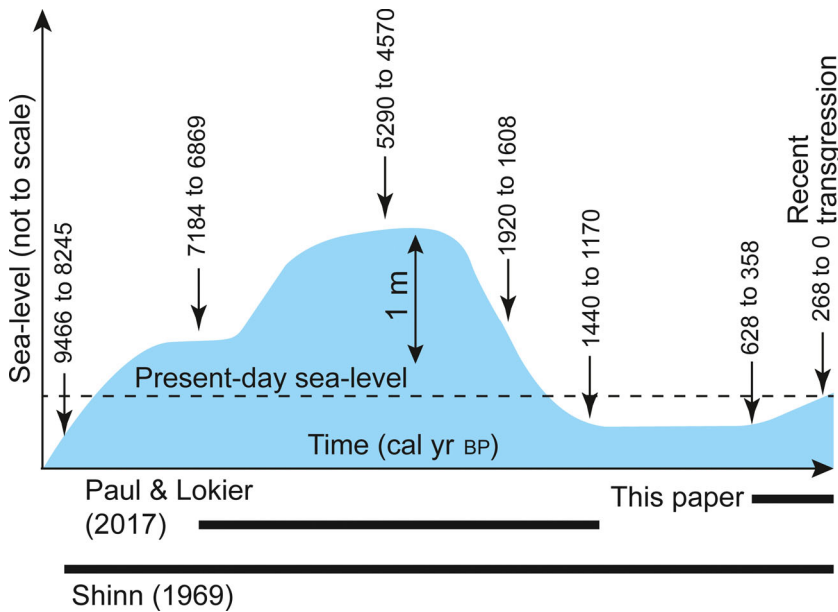
Fig. 11. Compilation of the dated cemented intervals from various studies (Shinn, 1969; Paul & Lokier, 2017; this study), and their relation to sea-level changes in the area. The sea-level curve is modified from Paul & Lokier (2017).

migrates landward during the currently rising sea level, but lithification may be active at the seafloor or some centimetres beneath the seafloor at the redox boundary. In the terminology of sequence stratigraphy, the firmgrounds to hardgrounds described here qualify as lithified transgressive lag deposits, or as high order 'parasequence boundaries' (in the sense of Catuneanu *et al.*, 2009; "...relative conformable successions of genetically related beds or bedsets bounded by a flooding surface..."). Where present, the facies across the parasequence boundary change from the coarser-grained lithified (packstone to rudstone) facies beneath to the unconsolidated silt-sized carbonate sediments above. In many places, however, the sediment on top of the actualistic (flooding) parasequence boundary has not yet been deposited. The early diagenetic cementation features in the Abu Dhabi coastal sabkha and lagoons are highly diverse. In the view of the authors, the wide spectrum of (sub)recent lithification features documented within the relatively small study area have no (preserved) analogue in the rock record. Below, five characteristic settings with cemented intervals are described and interpreted in the context of data compiled by the authors and previous workers.

*Actualistic firmgrounds in the intertidal Khawr Qantur coastal sabkha*

In the context of a Late Holocene regression that post-dates the relative highstand (5290 to 4570 cal yr BP; Fig. 11; Lokier *et al.*, 2015),

diachronous firmgrounds to hardgrounds form in the Khawr Qantur (KQ) intertidal sabkha (Table 3; Fig. 2D). These features were described in detail in Paul & Lokier (2017) and were interpreted as forced regression hardgrounds, overlying an older, transgressive hardground (7184 to 6869 cal yr BP). Radiocarbon ages of a gastropod from the seaward hardground site described in Paul & Lokier (2017) give a calibrated age of 0 to 256 cal yr BP (Lokier & Steuber, 2009). Complexity arises from the fact that these hardgrounds are diachronous (lithoclines *sensu* Purser, 1969) and one stage amalgamates with the following stage in either a seaward or landward direction.

Actualistic firmgrounds are brittle lithified crusts that form under the influence of rising relative sea level, stepping landward over sabkha sediments. Towards the upper limit of the intertidal zone, these firmgrounds thin and show patchy cementation suggesting that these are the most recent and incomplete stages of lithification. Seaward, the firmgrounds thicken, with increasing degrees of cementation, and are buried beneath thin layers of sediment.

Morphologically conspicuous, lath-shaped as well as columnar aragonite cements induce the lithification of peloidal sediments (Fig. 15). Often, individual crystals are covered by mucilaginous films, suggesting a link between microbial metabolism and early diagenetic lithification. Actualistic firmground cements described here differ from Middle to Late Holocene cemented intervals from the same transect, which

Fig. 12. Scanning electron microscope (SEM) images of various cement types from the Abu Dhabi lagoon and intertidal sabkha. (A) Micritic and rhombic high-Mg calcite cements within a bioclast chamber from the Khawr as Sadiyat (KAS) middle lagoon. (B) Polygonal gypsum cements covering a grain surface from the KAS middle lagoon. (C) Acicular aragonitic cement covering oolitic and peloidal sediment from the KAS outer lagoon. Note the microbial filaments. (D) Acicular (needle) aragonitic cements from the high-energy settings of the Al Gharbia (AG) inner lagoon. (E) Outer KAS lagoon fibrous aragonitic cements, with associated microbial filaments (arrowed). (F) Fibrous aragonitic cements with small holes at the termination, Khawr Qantur (KQ) inner lagoon. (G) KAS inner lagoon cements showing elongated prismatic aragonite cements with voids at the (001) (termination) surface. (H) Platy aragonitic cements associated with framboids in the KAS inner lagoon.
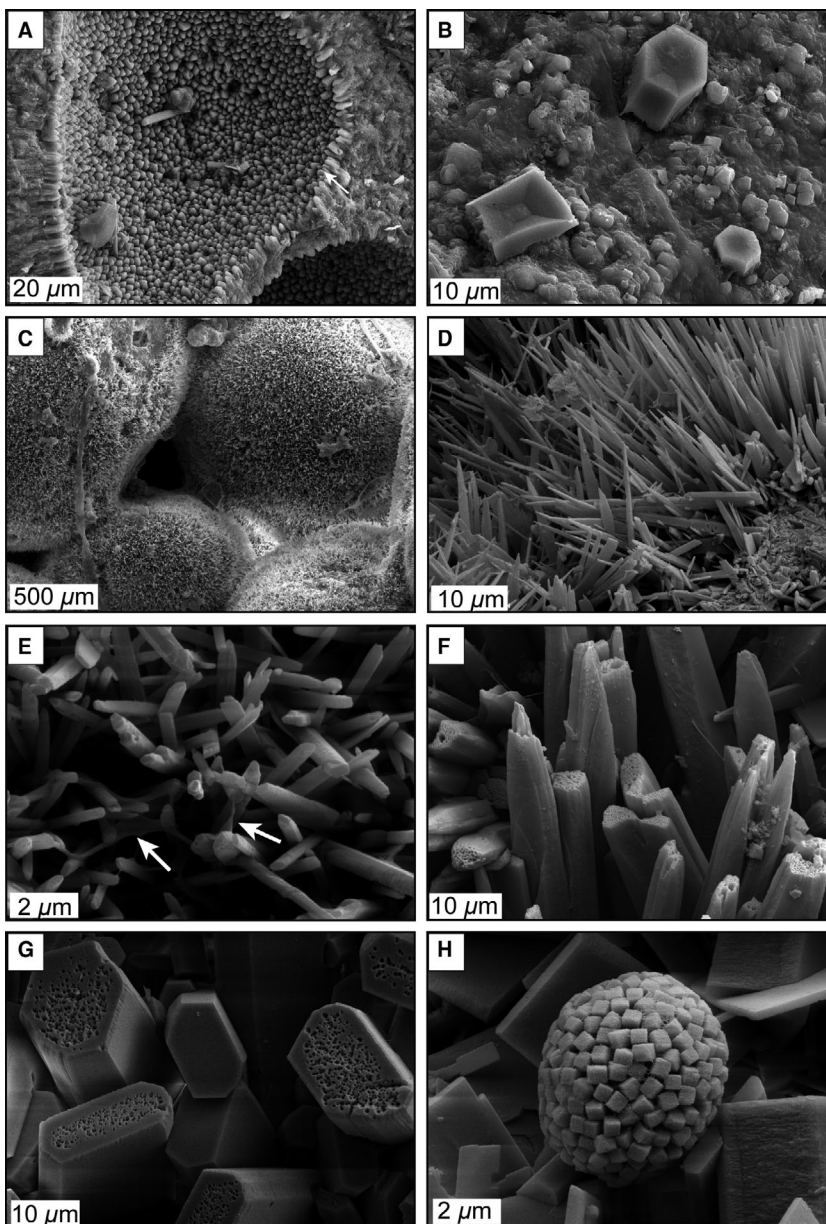
contain a more diverse mineralogy, including acicular aragonites, dog-tooth high Mg-calcites, as well as (non-stoichiometric) dolomite rhombohedra (Paul & Lokier, 2017). It seems likely that the observed differences in cement parageneses describe an evolution of hardground cementation over time, with the initial stage documented here (KQ transect in Fig. 2D) and more advanced stages described in Paul & Lokier (2017).

The KQ case examples document the highly complex firmground to hardground dynamics in a sabkha intertidal setting exposed to high-frequency, low-amplitude sea-level change. The result is a diachronous pattern of lithified surfaces that may amalgamate both seaward and landward. Supersaturated seawater with respect to aragonite, tide-induced water circulation, evaporation during low tide and microbial activity induce precipitation of aragonite cements and subordinate calcite and gypsum cements. The characteristically mammillated and irregular upper surfaces of the brittle firmgrounds developed in this environment are indicative of low hydrodynamic level. It is acknowledged that the level of research presented here, and in previous papers, is insufficient to capture the complexity of firmground in the intertidal sabkha of Abu Dhabi. Previous work dealing with microbe–
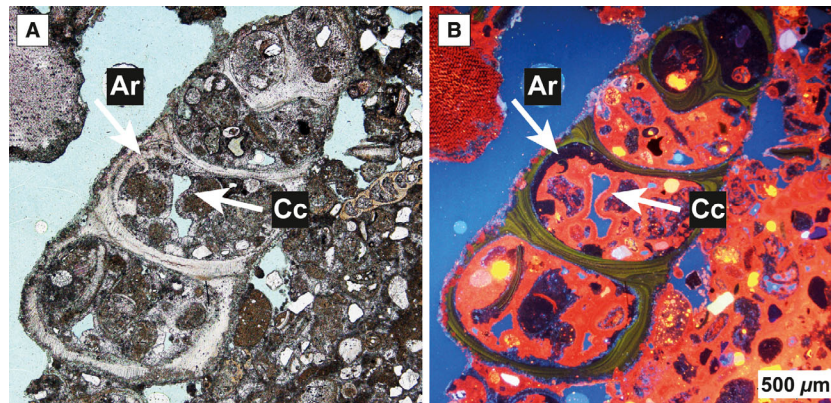
Fig. 13. Thin section images (plane polarized light) from Khawr as Sadiyat (KAS) middle lagoon. (A) Gastropod encased in firmground. Note aragonite (fibrous, Ar) and calcite (micritic, Cc) cements coating the shell interior and encasing sediment. (B) As (A) but under cathodoluminescence. Note green luminescence colour of gastropod shell, purple to dark red (Ar) cement fringes and bright orange micritic cement. In this specific sample, micrite cement forms up to 50% of all early marine cement phases. Micrite cement rests on shell material, aragonite cements and sediment. Remarkably, less than 10 ppm Mn^{2+} in the crystal lattice of calcitic sediments and cement are sufficient to induce bright orange luminescence in these actualistic sediments and cements.
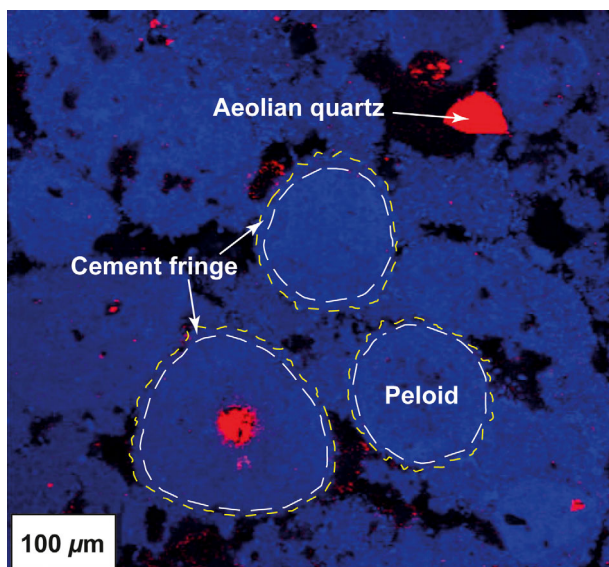
Fig. 14. Raman microscopy scan of a hardground from the Khawr as Sadiyat (KAS) inner lagoon documenting the aragonitic nature of the bulk of hardground cements. Aragonite is indicated by the blue colour, porosity is indicated by black and quartz is indicated by red. Primarily, round grains are composed of aragonite, with the exception of the quartz at the bottom left. White dashed lines indicate the grain boundaries, whereas yellow dashed lines indicate the edge of the fringing aragonitic cements.

sediment interaction in this area has mainly focused on the formation of highest Mg-calcite and non-stoichiometric dolomite in sabkha sediment (e.g. Bontognali *et al.*, 2010). In contrast, the role of biofilms on firmground aragonite and micritic Mg calcite cement nucleation and precipitation in the intertidal sabkha is underexplored. These features call for a study combining geomicrobiological, sedimentological and carbonate geochemical expertise.

Concretionary (sub)hardgrounds in the Khawr as Sadiyat inner lagoon

Shallow lagoonal cemented intervals in the innermost portion of the Khawr as Sadiyat (KAS) transect (Table 3; Fig. 2B) have been ^{14}C dated to 268 to 0 cal kyr BP to Recent. Encrustation or borings by endolithic organisms such as serpulids, bivalves or sponges (Fig. 7C), a feature typical for many of the firmgrounds to hardgrounds elsewhere in the Abu Dhabi lagoon, are lacking. In the literature, the absence of hardground encrustation and of endolithic borings are often taken as evidence of very short hiatal durations (Kennedy & Garrison, 1975). The case example documented here attests to the complexity of these processes. These brittle layers are overlain by some centimetres of fine-grained sediment and millimetre-thick microbial layers at the seafloor. No evidence is found that these features, characterized by conspicuously planar upper surfaces, represent conventional lithified seafloors subsequently buried under a shallow sediment cover.

A further conspicuous feature of these layers is the platy to columnar morphology of the
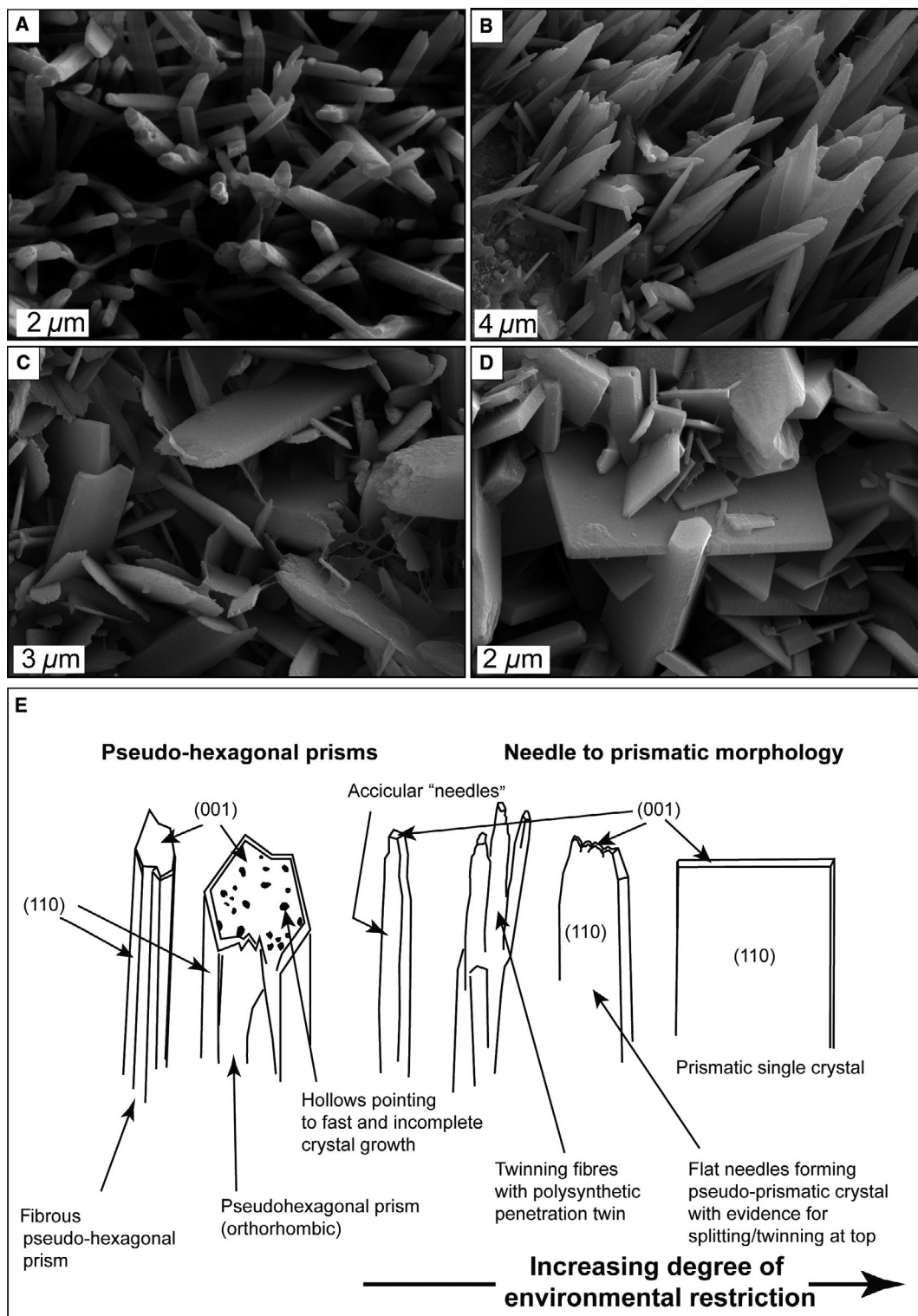
Fig. 15. Aragonitic cement morphologies from the Khawr as Sadiyat (KAS) lagoon. (A) Acicular cements in the outer lagoon. (B) Acicular cements showing twinning from the outer lagoon [but landward of (A)]. (C) Platy cements with pseudo-prismatic terminations from the inner lagoon. (D) Well-defined platy cements in the inner lagoon. (E) Sketch illustrating various cement fabrics as shown in SEM photographs (A) to (D). Trend from elongated pseudo-hexagonal fibers to prisms shown to the left. Trend from needle and fibrous to platy cements shown to the right. Degree of environmental restriction increases to the right. Note that the complexity of parameters that induce these morphological changes are not yet well understood.
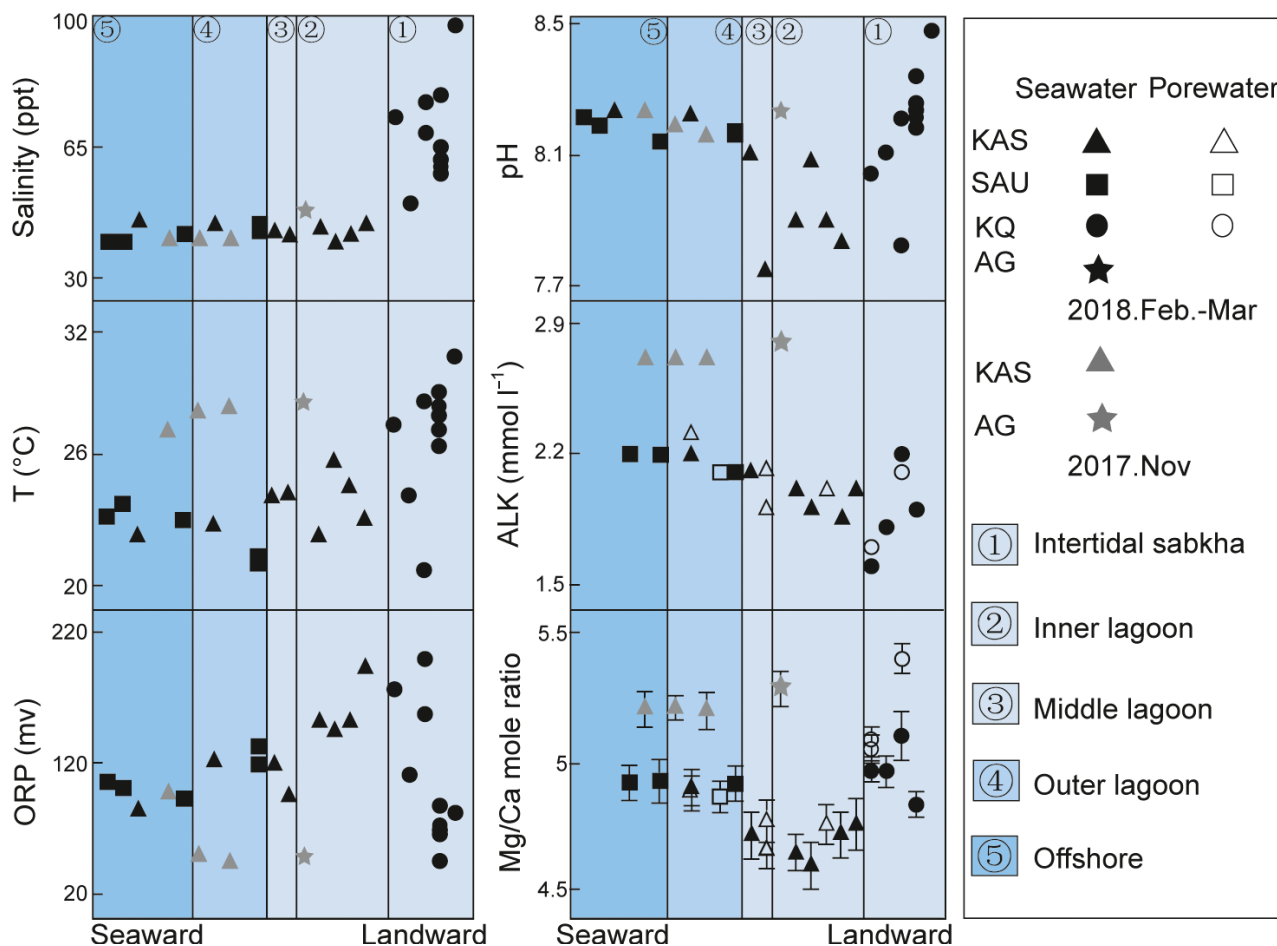
Fig. 16. Surface seawater and porewater properties along studied transects: ALK, alkalinity; ORP, oxidation-reduction potential.

aragonite cements. Rarely described in the literature, these cements lithify the carbonate sands (Figs 12 and 15). Numerous pyrite framboids (i.e. spherical aggregates of FeS_2 microcrystallites; Rickard, 1970) are embedded between these crystals (Fig. 12H). Several papers have discussed the level of complexity surrounding framboid formation and diagenesis (Sawlowicz, 1993; Wilkin & Barnes, 1997). Nevertheless: (i) the small size of the framboids (5 to 10 μm) suggests H_2S-bearing, oxygen-depleted pore waters (Wignall & Newton, 1998); and (ii) the presence of microbial communities in the inner lagoon provides a supply of abundant organic matter and may indicate a relation between microbial metabolisms and framboid formation.

Judging from field observations, the porewater redox boundary, situated about 15 to 20 cm beneath the seafloor (Fig. 6B), defines the upper limit of concretionary layers and may explain the uncommonly planar upper surface of these features. Interestingly, Pleistocene counterparts of the Khawr as Sadiyat inner lagoon (sub)hardgrounds are exposed due to channel construction work a few kilometres landward of the KQ transect. These display very similar, albeit fossil, examples of these concretionary sub-hardgrounds (Fig. 17).

With reference to the actualistic lithified intervals, cementation within the sediment column is possibly due to bacterial sulphate reduction (BSR; Berner, 1981). In this process, bicarbonate (HCO_3^-) is produced and, when deprotonated, it forms CO_3^{2-}. Given the abundance of Ca, an increase of alkalinity and porewater supersaturation with respect to $CaCO_3$ result, and the sulphate inhibitor is removed. The following generalized equation (see discussion in Petrash *et al.*, 2017) describes this process:
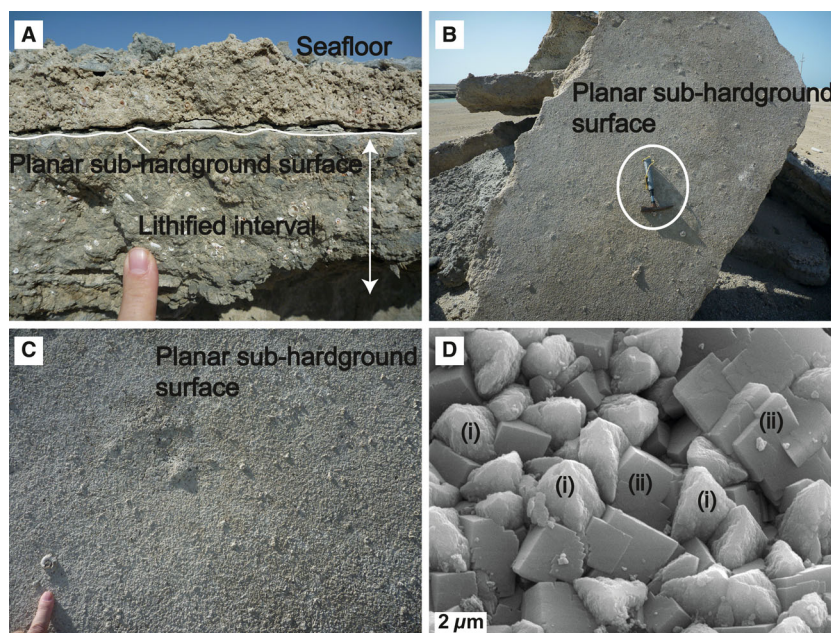
Fig. 17. Pleistocene hardground exposures due to channel-building activity to the south-east of the Khawr Qantur (KQ) transect. In the view of the authors, these features represent fossil representatives of the inner lagoon concretionary sub-hardgrounds (Fig. 7C). (A) Section of concretionary planar sub-hardground covered by *ca* 15 cm of poorly lithified sediment. Finger is 2 cm wide. (B) Sub-hardground surface exposed along channel. Note the extremely planar upper surface. Hammer for scale, 30 cm long. (C) Close up of (B). Serpulid to lower left is not encrusting but a component of the lithified interval. Finger is 2 cm wide. (D) Scanning electron microscope (SEM) image of cement phase lithifying Pleistocene sub-hardgrounds. Two cement phases are visible: (i) a corroded calcite phase; replaced by (ii) newly forming calcite rhombohedra. It seems likely that these calcites formed as a result of meteoric diagenesis and calcite to aragonite transformation.

$$CH_3COO^- + SO_4^{2-} + H_2O \rightarrow H_2S + 2HCO_3^- + OH^-$$
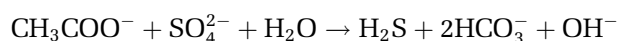
As a consequence, beneath the redox boundary aragonite and high-Mg calcite cementation from pore fluids with high Mg:Ca ratio take place. Under the hot arid climate in the Gulf, the surficial porewater is evaporated during low tide exposure of the inner lagoonal carbonate seafloor, inducing additional oversaturation (Noble & Howells, 1974) with respect to carbonate.

Moreover, oxidation of organic matter in the uppermost oxic sediment column generates CO_2, which in turn, causes the pH to decrease and porewater may become undersaturated with respect to more soluble carbonates such as aragonite (see discussion in Swart, 2015). With respect to ubiquitous aragonite cement precipitation beneath the redox boundary, the following considerations are relevant: the formation of early diagenetic concretionary nodules in the upper sediment column has been reported from numerous Holocene and older case examples (see Mullins *et al.*, 1980, for a discussion of Holocene carbonate nodules). Dissolution of (primarily)

aragonite occurs within the oxic zone of surficial sediment by oxidation of organic matter. Cement precipitation in the pore space within the upper sediment column results from the mixing of different hydro-chemical zones including the iron-reducing zone, downward diffusion of Ca^{2+} and bicarbonate, and increased alkalinity due to hydrogen consumption by iron reduction (Coimbra *et al.*, 2009). All of these factors are in agreement with the working hypothesis proposed here. Moreover, the high Mg:Ca pore fluid ratios may inhibit high-Mg calcites to pass the nucleation boundary and thus explain the dominance of aragonite cements (Morse *et al.*, 1997).

Geochemical fingerprints for either BSR or deeper-seated methanogenesis (Berner, 1981) are often found in characteristic $\delta^{13}C$ values (Games *et al.*, 1978). Given that the aragonitic cements are a volumetrically minor component of bulk samples, isotope data compiled so far plot within the range of published marine carbon isotope data (2.6 to 4.3‰; Paul & Lokier, 2017) in the Abu Dhabi lagoon. The way forward is to apply spatially-resolved secondary ion mass spectrometry

(SIMS) analysis of all cement phases in these intervals. This is work in progress.

These processes discussed here are not sufficiently understood and must be the topic of spatially-resolved geochemical analysis, detailed porewater sampling and analysis spreading over one to several years combined with field monitoring experiments. This is work presently underway. Assuming that the above model is correct, the question arises of whether these cemented intervals qualify as genuine firmgrounds to hardgrounds or if they share more similarities with concretionary layers? It is proposed that this type of cemented interval should be referred to as 'concretionary sub-hardgrounds' because they are not previously described in the literature. Concretionary sub-hardgrounds are relevant as they may contribute to the discussion on the origin of some of the rhythmical shallow water limestone–marl alternations as discussed in Munnecke *et al.* (2001). Conventionally, these successions are assumed to record cyclic sedimentation linked to Milankovitch cycles. Data shown here, i.e. the early marine diagenetic formation of concretionary sub-hardgrounds, might be relevant in this context as here a process is at work that is apparently not related to orbital cycles. Moreover, concretionary sub-hardgrounds may eventually become exposed at the seafloor due to winnowing and removal of the overlying sediment. In the fossil record, exhumed concretionary sub-hardgrounds are then easily confused with genuine marine hardgrounds. An important difference is that exposed sub-hardgrounds do not represent a hiatal interval.

Al Gharbia inner-lagoon hardgrounds grading landward into incipient beachrocks

Discontinuous hardgrounds are exposed at the seafloor in some tens of metres wide belts around the Al Gharbia (AG) spit (Table 3; Figs 2D and 8). Seaward of this hardground belt, a few centimetre thick veneer of sediment covers the surface. The depositional environment is distinct from the KAS innermost lagoonal environment by its higher-energy wave-exposed setting and lower salinities (40 to 50 ppt; Fig. 16). In a seaward to beach transect, features rapidly change over only some tens of metres. Hardgrounds display thicknesses of >12 cm some 30 to 40 m seaward from the beach, diminishing to <1 cm in thickness in the upper intertidal and along the beach front (Fig. 8). Seaward, the black

coloured hardgrounds are subject to localized disintegration and fragmentation alternating with areas of intact hardground surfaces extending over many metres in all directions (Fig. 8D and E). Living encrusting organisms are relatively rare at the upper surface of the hardground (Fig. 8B); however, abundant clusters of living bivalves (predominantly *Brachidontes*) and numerous species of gastropods colonize the irregular topography of the lower hardground surface adjacent to fractures (Fig. 8C). Landward, these hardgrounds thin and disintegrate over a short distance into layers of fragmented intraclasts, 1 to 3 cm thick and 5 to 20 cm wide (Fig. 8E). These intraclasts are reworked and transported over short distances by means of waves and currents. Further up-beach, the intraclast layer grades into weakly-cemented carbonate sands (Fig. 8F) that qualify as incipient beachrock in the sense of Scoffin & Stoddart (1983). The hardground interval has likely formed in the recent past, but the present hydrodynamic level at the spit causes disintegration.

The AG hardgrounds provide an excellent case example showing how shoreline dynamics in the Abu Dhabi lagoon produce significant changes in hardground thickness, morphology and degree of lithification over short distances (Fig. 8G). Similar to lithification features observed in the KQ intertidal sabkha, coastal marine hardgrounds and intertidal beachrock must be considered as features that are gradational in nature, with beachrock deposits changing seaward into marine hardgrounds.

Khawr as Sadiyat middle to outer lagoon hardgrounds with eroded tepees

Intertidal, barren hardground surfaces with large polygonal cracks in the KAS middle to outer lagoon (Table 3; Fig. 9D) complement previous observations from locations *ca* 60 km to the ESE (Lokier & Steuber, 2009). The current study concurs with the interpretation of Lokier & Steuber (2009) and assumes here that the formation of polygons is the result of displacive carbonate sediment cementation occurring during low tidal levels when shallow ponds of evaporated seawater cover the low-relief lithified seafloor (Fig. 9D). The cementing phases include abundant micritic cements, as well as elongated aragonite cements. Evaporation drives the precipitation of carbonate cements, and occasionally reaches the threshold of gypsum precipitation (Fig. 12B). Carbonate grains embedded in

these hardgrounds show abundant dissolution and pitting features under SEM, likely resulting from rare rainfall events during low tidal level when these surfaces are subaerially exposed.

A series of important differences between the hardground polygons described in Lokier & Steuber (2009) and those documented here from the middle KAS lagoon exist.

1 The buckled polygonal margins described in Lokier & Steuber (2009), and from many ancient peritidal tepees worldwide (Assereto & Kendall, 1977), form a topographic relief with evidence of overlap and overthrusting. In contrast, the polygon borders described here are flat and eroded (Fig. 9D), likely due to abrasion of coarse-grained sediment moved by waves across the hardground surface. These discrepancies are probably due to the different hydrodynamic levels when comparing the inner lagoonal settings described in Lokier & Steuber (2009) and the more exposed environment described here. Evidence for the punctuated high hydrodynamic levels (gale-force, north-west Shamal winds) is the coarse-grained nature of bioclastic debris and the presence of decimetre sized, rounded hardground lithoclasts that are found locally. The polygons described here are therefore considered to be eroded tepee hardgrounds.

2 A cross-section of the hardground layers is exposed at the eroded, downward-narrowing polygonal cracks in the middle lagoon. A recent stage of subvertical cement crusts coats the polygon borders, and coarse-grained sediments fill the remaining pore space (Fig. 9D).

3 The polygonal hardgrounds described in Lokier & Steuber (2009) are covered by several centimetres of unconsolidated sediment, whereas the hardgrounds observed here are exposed.

The polygonal hardgrounds from the KAS middle lagoon, as well as in Assereto & Kendall (1977) and in Lokier & Steuber (2009), share important similarities with the 'megapolygons' or 'giant polygons' from many case examples including: Triassic age hardgrounds in the Dolomites, Jurassic examples from Morocco, or Permian deposits from the Guadalupe Mountains (all in Assereto & Kendall, 1977). The comparison of Recent megapolygons in the Gulf with ancient tepee features is perhaps one of the rare examples of a genuine actualistic key to geological processes from the distant past.

Two lines of evidence are instrumental in the presented model.

1 The lithified sediments forming the hardgrounds in the middle lagoon are conspicuously coarse-grained, mud-lean rudstones with pore space largely occluded by aragonitic cements. Contrastingly, the sediments directly underlying and overlying the cemented interval are carbonate muds with a silt-fraction of skeletal debris, peloids and benthic foraminifera. Large skeletal components are less common and are likely washed in during storms. The concentration of coarser material in the cemented interval is evidence for a localized increase in hydrodynamic level and sediment winnowing.

2 The presently-exposed hardground belt coincides with the low-tide level. The shallow effective wave base (some tens of centimetres deep) directly interacts with the seafloor and visibly entrains fine-grained material that is then transported into deeper water. Seaward of this facies belt, the hardground thickens and is covered by unconsolidated carbonate sediment (Fig. 9). The latter feature is consistent with the middle lagoonal outcrop belt being displaced landward during ongoing relative sea-level rise.

The zone of the mean high-tide level acts as a zone of increased energy and incipient hardground formation during windy days. Arguments for this come from the well-washed, rounded carbonate arenites along the rocky shoreline of the inner middle lagoon. Occasional storms could denude the incipient hardground and trigger a pulse of lithification. A subsequent decrease in hydrodynamic level would cause these firmgrounds to become covered by a thin sediment veneer transported by tidal current and fair-weather wave activity.

Sub-recent, cemented burrows in the Khawr as Sadiyat inter-shoal area

The ooid shoal belt is a typical feature of the outer Abu Dhabi lagoon, and forms the seaward limit of the Khawr as Sadiyat transect (KAS in Fig. 2B). Here, lithified decapod burrows occur in the shallow, permanently subtidal areas between active ooid shoals, of which the tops become exposed during low tide (Fig. 5C and D). Radiocarbon age dating of *Brachidontes* bivalve shells indicates a range between 628 cal yr BP and 358 cal yr BP. It is unclear whether the sub-recent lithified decapod burrow intervals form the substratum over which ooid shoals migrate, or if these represent features that form exclusively in the stabilized intershoal areas (Fig. 10A and B). As the ooid shoals

migrate during tidal fluctuations and under wave action, the lithified burrow intervals are buried by the ooidal sands, and other burrow networks are exposed (Fig. 10B). An attempt to dig a trench from the top of an active ooid shoal downward to what might be the lithified burrow interval underneath failed as the sides of the trench are highly unstable and constantly collapse. The burrow networks are mainly composed of ooids, cemented by the typical acicular aragonite needles (Fig. 12C) described from many locations in the (sub)tropical domain (Harris, 1978; Dravis, 1979; Strasser *et al.*, 1989).

The lithified decapod burrows that form patchy cemented intervals in the intershoal environment are rather peculiar case examples of early marine lithification. Due to the combination of burrowing organisms, microbe–sediment interaction, hydrodynamics and seawater geochemistry (see discussion in Rameil, 2008) the processes of cementation are likely complex. In the pore-fluids that fill these burrows, a microenvironment, that is also linked to specific bacterial consortia in the faecal pellets of decapods and the organic burrow lining, may facilitate cementation (Mirsal & Zankl, 1985). Judging from field observations, lithified burrows act as a substratum for further lithification of inter-burrow sediments resulting in irregular, tabular cemented intervals that do not qualify as surficial marine hardgrounds but may be more closely related to the concretionary sub-hardgrounds described from the Khawr as Sadiyat inner lagoon, even if the mechanisms involved are very different.

Factors controlling aragonite cement morphology

Complex morphological patterns found in aragonite overgrowth cements, similar to those observed across the transects described here, have only been described in a very limited number of previous studies (Schroeder, 1972; Strasser & Strohmenger, 1997). However, the unspecified reference to aragonitic lath-cements is found throughout the literature. The most detailed description is from Schroeder (1972), who referred to 'board-shaped' crystals with some rods and laths from Holocene algal cup reefs in Bermuda. Schroeder (1972) also briefly discussed cementation factors and concluded that no systematic relation between cement mineralogy, morphology and environmental factors exists.

Despite a high level of local complexity in the cement morphologies, the following first-order pattern is observed: needle-shaped and acicular aragonite cements typify the outer lagoonal settings. No further discussion is provided here because description of these fabrics in the literature is extensive. In the middle to inner lagoon, aragonite cement morphologies range from needle-shaped to flattened needles (fibrous cements), to bifurcating arrays of fibrous cements (Fig. 15A to D). These co-exist with elongate pseudo-hexagonal aragonite prisms. The peloidal sands that accumulate along the shoreline in the upper tidal domain and the intertidal sabkha display various degrees of cementation with platy aragonite crystals. A tentative succession of aragonite cements with needles at one end of the spectrum, and platy and columnar morphologies at the other end of the spectrum is shown in Fig. 15E.

It is emphasized that the environmental factors that affect the various aragonite cement morphologies are most likely complex and so is, when studied in detail, their spatial distribution along the proximal to distal transects. The first order spatio-environmental pattern, however, with needle-like aragonites in the normal marine, wave agitated outer lagoon, gradually changing to more flattened morphologies in the middle lagoon and the dominance of platy and columnar morphologies in the inner-mid lagoon to sabkha, is well-constrained. In agreement with fundamental principles in crystallography, the various morphologies result from variations in the growth rate of specific crystal surfaces and the interaction of inhibitors with some of these surfaces. Needle cements are typified by growth perpendicular to the (001) surface (base and top), with (110) surfaces (sides) being poorly developed (Fig. 15A), typical for crystals with very high growth rates (Given & Wilkinson, 1985). The increasing degree of flattening of needles to form fibres and the development of arrays of bifurcating needles are the result of more pronounced, but still suppressed, growth of one of the (110) crystal surfaces (Fig. 15B and C). The platy and columnar morphologies, best developed in the poorly-lithified peloidal sands in the inner, middle lagoon and intertidal sabkha (Fig. 15D), share similarities with single crystals that lack twinning but display a well-developed orthorhombic morphology. It seems likely that, here, crystal growth along the (001) surface is not significantly different from that along other surfaces.
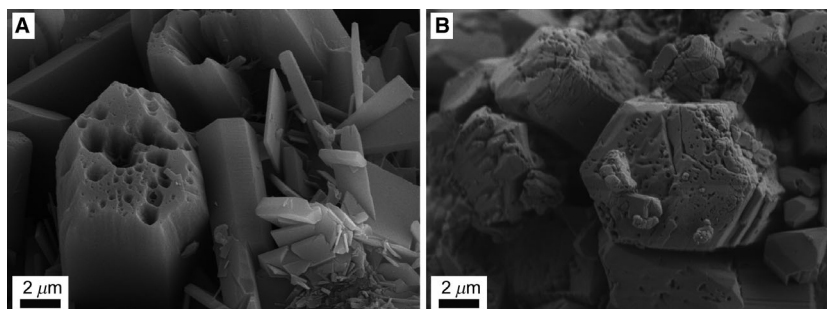
The characteristic elongated pseudo-hexagonal prisms (Fig. 12G) result when the orthorhombic

aragonites show poorly-developed twinning. An interesting feature found is the V-shaped, irregular pits that characterize the upper (001) surface yet are absent at other crystal surfaces. Based on experimental work (Goetschl *et al.*, 2019), the most likely explanation for these features is the adsorption of inhibitors (hydrated Mg^{2+} ions, PO_4^{3-}, SO_4^{2-}) with the fast growing (001) crystal surface or organic constituents [microbial extracellular polymeric substances (EPS), amino acids; Chave & Suess, 1970; Berner, 1975; Burton & Walter, 1990; Burton, 1993; Lin *et al.*, 2005]. At the site of cation attachment, aragonite cementation is temporarily inhibited, resulting in hollows that later become 'healed' when $CaCO_3$ resumes.

In the context of inorganic precipitation experiments (Goetschl *et al.*, 2019), elongated aragonite prisms with hollows in their (001) surface formed and share remarkable similarities with some of the aragonite cements found in the concretionary (sub)hardgrounds described here (Fig. 18). Acknowledging that laboratory precipitation experiments are only in part analogues of natural diagenetic environments, the following tentative conclusions can be drawn; evidence was found that the porous crystal surface structure of the precipitated aragonite (Fig. 18) was caused by active blocking of crystal growth sites due to adsorption phenomena. Foreign ions including SO_4^{2-} and Mg^{2+} or their aqueous complexes (for example, $CaSO_4^0$ and $MgSO_4^0$) that are present in the reactive solution can adsorb on mineral growth sites and may occupy the active surface area of growth. Consequently, new molecules cannot adapt at the surface and crystal growth is disturbed, similar as previously observed for calcite (Reddy & Wang, 1980; Katsifaras & Spanos, 1999; Goetschl *et al.*, 2019). Adsorption of aqueous species on the crystal surface is controlled by dynamic exchange equilibrium and assures that no surface site is blocked permanently. Further, the uncommon aragonite morphologies are not necessarily the product of, for example, microbe–mineral interaction but form due to specific characteristics of porewater chemistry and crystal nucleation and precipitation kinetics.

When considering the differences in seawater properties between the intertidal sabkha and inner lagoon, the intertidal sabkha generally has higher temperature, salinity, alkalinity and pH, resulting in higher dissolved solids but a lower redox potential relative to the middle and outer lagoons (Fig. 16). The high Mg/Ca fluid ratios (>5; Fig. 16) from which platy aragonite cements precipitate in the intertidal sabkha contrast with the classical work of Folk (1974), which suggested that high rates of crystallization and high Mg/Ca ratios will precipitate fibrous crystals, while low rates of crystallization and low Mg/Ca ratios correspond to coarser and equant crystals. However, lower Mg/Ca ratios in the inner lagoon also result in platy morphologies indicating that other mechanisms are at work. The investigation of aragonite cement types in an environmental context seems promising; however, identifying the morphology-controlling factors among the many parameters within each environment remains difficult. A potential way forward may include combining detailed field monitoring with additional and well-calibrated laboratory precipitation experiments.

Fig. 18. Elongated pseudo-hexagonal aragonite prisms. (A) Aragonite cement from Khawr as Sadiyat (KAS) inner lagoon sub-hardgrounds. Note the characteristic pits at (001) surface. (B) Aragonite cement precipitated in the context of abiogenic experimental work (Goetschl *et al.*, 2019). Scanning electron microscope (SEM) image of pseudo-hexagonal aragonite prism with prominent porous surface structure. Aragonite was precipitated at a mineral growth rate of about $10^{-7.2}$ mol m^{-2} s^{-1} and in the presence of 30 mM sulphate.

Constraints on the high-Mg calcite and aragonite dichotomy

The dominant carbonate cement phase in cemented intervals found in the lagoon and intertidal sabkha of Abu Dhabi is aragonite. In the inner lagoon and the intertidal sabkha, however, micritic high-Mg calcite may locally constitute 10 to 50 vol.% of all cement fabrics (based on thin section evidence). The question that what drives aragonite versus calcite cement precipitation from marine porewaters endures (Friedman *et al.*, 1974). In the context of this study, two main controlling factors are proposed that may, at least in part, explain the dominance of aragonite cements.

1 In aragonitic host sediment, such as the case in the ooid shoals of the outer lagoonal setting, aragonite needle cements preferentially nucleate on aragonite (ooid) substrata. Quantitative data for the effect of substratum (seed) mineralogy on the mineralogy of cements that nucleate on these surfaces come from experimental work (Lin *et al.*, 2005), but evidence is also documented from various recent carbonate precipitation experiments including those involving caves (Riechelmann *et al.*, 2014).

2 The formation of the crystal nuclei from a parent fluid takes place on a nano-scale or sub-nano-scale and is a dynamic process dictated by minimizing the Gibbs free energy. Smaller nuclei have the tendency to dissolve shortly after their formation because of their large free energy caused by the large surface to volume ratio (Zhang & Liu, 2009). Those among the nuclei, however, that cross the nucleation barrier and reach a critical radius, reach overall lower free energy and precipitation takes place. The nucleation barrier is dependent on the structure and mineralogy of nuclei as well as on the degree of supersaturation and chemistry of the parent fluid. According to the classical nucleation theory, the structure of the nuclei is the same as that of the stable phase (Fokin *et al.*, 2005). At high fluid Mg/Ca ratios, as is the case in porewater settings studied here, both aragonite and high-Mg calcite nuclei form. Given that Mg in the crystal structure of $CaCO_3$ increases the free energy of the calcite nuclei, many of these magnesian calcite nuclei may not cross the nucleation barrier and dissolve. Moreover, adsorption of Mg^{2+} and SO_4^{2-} may inhibit calcite growth. In contrast, the Mg-lean aragonite nuclei commonly reach lower free energy levels and may grow to form abundant cement rinds.

A higher level of complexity is found in some of the samples taken from lagoonal and intertidal sabkha cemented intervals. There, locally, high-Mg calcite (micritic cement) may be volumetrically more important. The observation that two samples, collected only metres apart in the same cemented interval, may yield very different aragonite–calcite cement ratios and points to the significance of local chemical microenvironments that are not yet well understood.

CONCLUSIONS

Combining laboratory data and direct observations of modern cemented intervals (beachrock, firmgrounds to hardgrounds and concretionary features) from the lagoon and intertidal sabkha of Abu Dhabi, the following conclusions are drawn.

Radiocarbon ages suggest that seafloor lithification commenced in the Middle to Late Holocene (about 9000 yr BP), and proceeds to the present-day. Holocene and Recent hardgrounds likely amalgamate in places. Transgressive and regressive relative sea-level changes across the extremely low-angle (<0.1°) carbonate ramp shift the coastline and the zone of wave base–seafloor interaction, either seaward or landward, and induce the precipitation of aragonite, (micritic) calcite, and less commonly, gypsum cements. Given the present-day relative sea-level rise transgressing over the Abu Dhabi sabkha, the cemented intervals studied here are interpreted as actualistic parasequence boundaries in the sense of a marine flooding surface.

The diversity of lithification features in the comparably small study area in Abu Dhabi is bewildering and testifies to the value of actualistic study areas to understand and interpret early diagenetic seafloor lithification in the geological past. Particular relevance of this study lies in the predominantly aragonite-cemented nature of these intervals, which have limited preservation potential in the rock record. Only locally, high-Mg calcites may form up to 50% of the cement phase. Reasons for the aragonite-dominated mineralogy of early diagenetic cements may include substratum effects and the fact that many high-Mg calcite nuclei may not cross the nucleation barrier and dissolve. Early diagenetic lithification actively occurs in: (i) open, current-swept channels of the outer lagoon, in low-lying areas between ooid shoals; (ii) at the seafloor and some centimetres beneath the inner lagoonal seafloor in the intertidal zone of the middle to inner lagoon (i.e.

within the sediment column); and (iii) at the inter-tidal sabkha.

The morphology of aragonitic hardground cements ranges from needle-shaped (in the outer lagoon) to complex columnar, lath and platy crystals (in the inner middle lagoon to the intertidal sabkha) that have only rarely been described in the literature. A direct relation between aragonite cement morphology, lithification mechanisms and degree of environmental restriction is proposed at the level of a tentative working hypothesis. Inorganic precipitation experiments produce elongated pseudo-hexagonal aragonite prisms similar to those found in the inner lagoon and intertidal sabkha and suggest the significance of high fluid Mg/Ca ratios and sulphate.

Many of the features documented here are not well-explained by existing models of hardground formation. Coastal marine hardgrounds and beachrock lithification may be transitional with beachrock intervals grading seaward into marine hardgrounds. The term 'concretionary sub-hardground' is introduced for lithification features within the sediment column that may qualify as planar concretionary layers *sensu lato* rather than as firmgrounds. Data and observations shown here may have relevance for the interpretation of rhythmical shale–limestone alternations conventionally assigned to Milankovitch patterns, palaeoenvironmental research and the recognition and interpretation of ancient aragonite-cemented hardgrounds.

ACKNOWLEDGEMENTS

DATA AVAILABILITY STATEMENT

The data that support the findings of this study are available from the corresponding author upon reasonable request.

REFERENCES

Assereto, A.L. and **Kendall, C.G.St.C.** (1977) Nature, origin and classification of peritidal tepee structures and related breccias. *Sedimentology*, **24**, 153–210.

Bathurst, R.G.C. (1975) Diagenesis on ancient sea floors. In: *Carbonate Sediments and their Diagenesis, Development in Sedimentology* (Ed. Bathurst, R.G.C.), pp. 395. Elsevier, New York.

Berner, R.A. (1975) The role of magnesium in the crystal growth of calcite and aragonite from sea water. *Geochim. Cosmochim. Acta*, **39**, 489–504.

Berner, R.A. (1981) A new geochemical classification of sedimentary environments. *J. Sed. Petrol.*, **51**, 359–365.

Bontognali, T.R.R., **Vasconcelos, C.**, **Warthmann, R.J.**, **Bernasconi, S.M.**, **Dupraz, C.**, **Strohmenger, C.J.** and **McKenzie, J.A.** (2010) Dolomite formation within microbial mats in the coastal sabkha of Abu Dhabi (United Arab Emirates). *Sedimentology*, **57**, 824–844.

Brett, C.E. and **Brookfield, M.E.** (1984) Morphology, faunas and genesis of Ordovician hardgrounds from southern Ontario, Canada. *Palaeogeogr. Palaeoclimatol. Palaeoecol.*, **46**, 233–290.

Burton, E.A. (1993) Controls on marine carbonate cement mineralogy: review and reassessment. *Chem. Geol.*, **105**, 163–179.

Burton, E.A. and **Walter, L.M.** (1990) The role of pH in phosphate inhibition of calcite and aragonite precipitation rates in seawater. *Geochim. Cosmochim. Acta*, **54**, 797–808.

Catuneanu, O., **Abreu, V.**, **Bhattacharya, J.P.**, **Blum, M.D.**, **Dalrymple, R.W.**, **Eriksson, P.G.**, **Fielding, C.R.**, **Fisher, W.L.**, **Galloway, W.E.**, **Gibling, M.R.**, **Giles, K.A.**, **Holbrook, J.M.**, **Jordan, R.**, **Kendall, C.G.St.C.**, **Macurda, B.**, **Martinsen, O.J.**, **Miall, A.D.**, **Neal, J.E.**, **Nummedal, D.**, **Pomar, L.**, **Posamentier, H.W.**, **Pratt, B.R.**, **Sarg, J.F.**, **Shanley, K.I.W.**, **Steel, R.J.**, **Strasser, A.**, **Tucker, M.E.** and **Winker, C.** (2009) Towards the standardization of sequence stratigraphy. *Earth Sci. Rev.*, **92**, 1–33.

Chave, K.E. and **Suess, E.** (1970) Calcium carbonate saturation in seawater: effects of dissolved organic matter. *Limnol. Oceanogr.*, **15**, 633–637.

Christ, N., **Immenhauser, A.**, **Wood, R.**, **Darwich, K.** and **Niedermayr, A.** (2015) Petrography and environmental controls on the formation of Phanerozoic marine carbonate hardgrounds. *Earth Sci. Rev.*, **151**, 176–226.

Clari, P.A., **Della Pierre, F.** and **Martire, L.** (1995) Discontinuities in carbonate successions: identification, interpretation and classification of some Italian examples. *Sed. Geol.*, **100**, 97–121.

Coimbra, R., **Immenhauser, A.** and **Olóriz, F.** (2009) Matrix micrite δ^{13}C and δ^{18}O reveals synsedimentary marine lithification in Upper Jurassic Ammonitico Rosso limestones (Betic Cordillera, SE Spain). *Sed. Geol.*, **219**, 332–348.

De Boever, E., **Brasier, A.T.**, **Foubert, A.** and **Kele, S.** (2017) What do we really know about early diagenesis of non-marine carbonates? *Sed. Geol.*, **361**, 25–51.

Dickson, J.A.D. (1965) A modified staining technique for carbonates in thin section. *Nature*, **205**, 587.

Dravis, J. (1979) Rapid and widespread generation of Recent oolitic hardgrounds on a high energy Bahamian platform, Eleuthera Bank, Bahamas. *J. Sed. Res.*, **49**, 195–207.

El-Sayed, M.I. (1999) Sedimentological characteristics and morphology of the aeolian sand dunes in the eastern part

of the UAE: a case study from Ar Rub' Al Khali. *Sed. Geol.*, **123**, 219–239.

Evans, G., Schmidt, V., Bush, P. and Nelson, H. (1969) Stratigraphy and geologic history of the sabkha, Abu Dhabi, Persian Gulf. *Sedimentology*, **12**, 145–159.

Fokin, V.M., Yuritsyn, N.S. and Zanotto, E.D. (2005) Nucleation and crystallization kinetics in silicate glasses: theory and experiment. In: *Nucleation Theory and Applications* (Ed. Schmelzer, J.W.P.), pp. 74–125. Wiley-VCH Verlag GmbH & Co. KGaA, Weinheim.

Folk, R.L. (1974) The natural history of crystalline calcium carbonate: effect of magnesium content and salinity. *J. Sed. Petrol.*, **44**, 40–53.

Föllmi, K.B. (2016) Sedimentary condensation. *Earth Sci. Rev.*, **152**, 143–180.

Friedman, G.M. (1959) Identification of carbonate minerals by staining methods. *J. Sed. Petrol.*, **29**, 87–97.

Friedman, G.M., Amiel, A.J. and Schneidermann, N. (1974) Submarine cementation in reefs: example from the Red Sea. *J. Sed. Petrol.*, **44**, 816–825.

Games, L.M., HayesRobert, J. and Gunsalus, P. (1978) Methane-producing bacteria: natural fractionations of the stable carbon isotopes. *Geochim. Cosmochim. Acta*, **42**, 1295–1297.

Given, R.K. and Wilkinson, B.H. (1985) Kinetic control of morphology, composition, and mineralogy of abiotic sedimentary carbonates. *J. Sed. Petrol.*, **55**, 109–119.

Goetschl, K.E., Purgstaller, B., Dietzel, M. and Mavromatis, V. (2019) Effect of sulfate on magnesium incorporation in low-Mg calcite. *Geochim. Cosmochim. Acta*, **265**, 505–519.

Harris, P.M. (1978) Holocene marine-cemented sands, Joulters ooid shoal, Bahamas. *Trans. Gulf Coast Assoc. Geol. Soc.*, **28**, 175–183.

Hattin, D.E. and Dodd, J.R. (1978) Holocene cementation of carbonate sediments in the Florida Keys. *J. Sed. Petrol.*, **48**, 307–312.

Holail, H. and Rashed, M. (1992) Stable isotopic composition of carbonate-cemented recent beachrock along the Mediterranean and the Red Sea coasts of Egypt. *Mar. Geol.*, **106**, 141–148.

Hughen, K.A., Baillie, M.G.L., Bard, E., Bayliss, A., Beck, J.W., Bertrand, C.J.H., Blackwell, P.G., Buck, C.E., Burr, G.S., Cutler, K.B., Damon, P.E., Edwards, R.L., Fairbanks, R.G., Friedrich, M., Guilderson, T.P., Kromer, B., McCormac, F.G., Manning, S.W., Bronk Ramsey, C., Reimer, P.J., Reimer, R.W., Remmele, S., Southon, J.R., Stuiver, M., Talamo, S., Taylor, F.W., van der Plicht, J. and Weyhenmeyer, C.E. (2004) Marine04: marine radiocarbon age calibration, 26–0 ka BP. *Radiocarbon*, **46**, 1059–1086.

Katsifaras, A. and Spanos, N. (1999) Effect of inorganic phosphate ions on the spontaneous precipitation of vaterite and on the transformation of vaterite to calcite. *J. Cryst. Growth*, **204**, 183–190.

Kennedy, W.J. and Garrison, R.E. (1975) Morphology and genesis of nodular chalks and hardgrounds in the Upper Cretaceous of southern England. *Sedimentology*, **22**, 311–386.

Khalaf, F., Milliman, J.D. and Druffel, E.M. (1987) Submarine limestones in the nearshore environment off Kuwait, northern Arabian Gulf. *Sedimentology*, **34**, 67–75.

Kinsman, D.J.J. (1964) Recent carbonate sedimentation near Abu Dhabi, Trucial Coast, Persian Gulf. PhD Thesis, The University of London, UK.

Lin, Y.P., Singer, P.C. and Aiken, G.R. (2005) Inhibition of calcite precipitation by natural organic material: kinetics, mechanism, and thermodynamics. *Environ. Sci. Technol.*, **39**, 6420–6428.

Lokier, S.W. (2013) Coastal Sabkha preservation in the Arabian Gulf. *Geoheritage*, **5**, 11–22.

Lokier, S.W. and Fiorini, F. (2016) Temporal evolution of a carbonate coastal system, Abu Dhabi, United Arab Emirates. *Mar. Geol.*, **381**, 102–113.

Lokier, S. and Steuber, T. (2009) Large-scale intertidal polygonal features of the Abu Dhabi coastline. *Sedimentology*, **56**, 609–621.

Lokier, S.W., Bateman, M.D., Larkin, N.R., Rye, P. and Stewart, J.R. (2015) Late Quaternary sea level changes of the Persian Gulf. *Quatern. Res.*, **84**, 69–81.

Lokier, S.W., Court, W.M., Onuma, T. and Paul, A. (2018) Implications of sea level rise in a modern carbonate ramp setting. *Geomorphology*, **304**, 64–73.

Marshall, J.F. and Davies, P.J. (1981) Submarine lithification on windward reef slopes: Capricorn-Bunker Group, southern Great Barrier reef. *J. Sed. Res.*, **51**, 953–960.

Mirsal, I.A. and Zankl, H. (1985) Some phenomenological aspects of carbonate geochemistry. The control effect of transition metals. *Geol. Rundsch.*, **74**, 367–377.

Molenaar, N. and Zijlstra, J.J.P. (1997) Differential early diagenetic low-Mg calcite cementation and rhythmic hardground development in Campanian-Maastrichtian chalk. *Sed. Geol.*, **109**, 261–281.

Morse, J.W., Wang, Q. and Tsio, M.Y. (1997) Influences of temperature and Mg: Ca ratio on $CaCO_3$ precipitation from seawater. *Geology*, **25**, 85–87.

Mullins, H.T., Neumann, A.C., Wilber, R.J. and Boardman, M.R. (1980) Nodular carbonate sediment on Bahamian slopes: possible precursors to nodular limestones. *J. Sed. Petrol.*, **50**, 117–131.

Munnecke, A., Westphal, H., Elrick, M. and Reijmer, J.J.G. (2001) The mineralogical composition of precursor sediments of calcareous rhythmites: a new approach. *Int. J. Earth Sci.*, **90**, 795–812.

Mutti, M. and Bernoulli, D. (2003) Early marine lithification and hardground development on a Miocene ramp (Maiella, Italy): key surfaces to track changes in trophic resources in nontropical carbonate settings. *J. Sed. Res.*, **73**, 296–308.

Nehrke, G. and Nouet, J. (2011) Confocal Raman microscopy as a tool to describe different mineral and organic phases at high spatial resolution within marine biogenic carbonates: case study on *Nerita undata* (Gastropoda, Neritopsina). *Biogeoscience*, **8**, 3761–3769.

Nehrke, G., Poigner, H., Wilhelms-Dick, D., Brey, T. and Abele, D. (2012) Coexistence of three carbonate polymorphs in the shell of the Antarctic clam *Laternula elliptica*. *Geochem. Geophys. Geosyst.*, **13**, Q05014.

Neumann, A.C. and Land, L.S. (1975) Lime mud deposition and calcareous and calcareous algae in the Bight of Abaco, Bahamas: a budget. *J. Sed. Petrol.*, **45**, 763–786.

Noble, J.P.A. and Howells, K.D.M. (1974) Early marine lithification of the nodular limestones in the Silurian of New Brunswick. *Sedimentology*, **21**, 597–609.

Paul, A. and Lokier, S.W. (2017) Holocene marine hardground formation in the Arabian Gulf: Shoreline stabilisation, sea level and early diagenesis in the coastal sabkha of Abu Dhabi. *Sed. Geol.*, **352**, 1–13.

Petrash, D.A., Bialik, O.M., Bontognali, T.R.R., Vasconcelos, C., Roberts, J.A., McKenzie, J.A. and Konhauser, K.O.

(2017) Microbially catalyzed dolomite formation: from near-surface to burial. *Earth-Sci. Rev.*, **171**, 558–582.

Purser, B.H. (1969) Syn-sedimentary marine lithification of Middle Jurassic limestones in the Paris Basin. *Sedimentology*, **12**, 205–230.

Purser, B.H. and **Evans, G.** (1973) Regional sedimentation along the Trucial Coast, SE Persian Gulf. In: *The Persian Gulf: Holocene Carbonate Sedimentation and Diagenesis in a Shallow Epicontinental Sea* (Ed. Purser, B.H.), pp. 211–232. Springer, New York.

Rameil, N. (2008) Early diagenetic dolomitization and dedolomitization of Late Jurassic and earliest Cretaceous platform carbonates: a case study from the Jura Mountains (NW Switzerland, E France). *Sed. Geol.*, **212**, 70–85.

Reddy, M.M. and **Wang, K.K.** (1980) Crystallization of calcium carbonate in the presence of metal ions. *J. Cryst. Growth*, **50**, 470–480.

Rickard, D.T. (1970) The origin of framboids. *Lithos*, **3**, 269–293.

Riechelmann, S., **Schröder-Ritzrau, A.**, **Wassenburg, J.A.**, **Schreuer, J.**, **Richter, D.K.**, **Riechelmann, D.F.C.**, **Terente, M.**, **Constantin, S.**, **Mangini, A.** and **Immenhauser, A.** (2014) Physicochemical characteristics of drip waters: influence on mineralogy and crystal morphology of recent cave carbonate precipitates. *Geochim. Cosmochim. Acta*, **145**, 13–29.

Sadrinasab, M. and **Kenarkohi, K.** (2009) Three-dimensional numerical modelling study of sound speed in the Persian Gulf. *Asian J. Appl. Sci.*, **2**, 232–239.

Sandberg, P.A. (1985) Aragonite cements and their occurrence in ancient limestones. In: *Carbonate Cements* (Eds Schneidermann, N. and Harris, P.M.). The Society of Economic Paleontologists and Mineralogists, Special Publication, 33–57.

Sawlowicz, Z. (1993) Pyrite framboids and their development: a new conceptual mechanism. *Geol. Rundsch.*, **82**, 148–156.

Schroeder, J.H. (1972) Fabrics and sequences of submarine carbonate cements in Holocene Bermuda cup reefs. *Int. J. Earth Sci.*, **61**, 708–730.

Scoffin, T.P. and **Stoddart, D.R.** (1983) Beachrock and intertidal sediments. In: *An Introduction to Carbonate Sediments and Rocks* (Eds Goudie, A.S. and Pye, K.), p. 400. Elsevier, San Diego.

Shinn, E.A. (1969) Submarine lithification of Holocene carbonate sediments in the Persian Gulf. *Sedimentology*, **12**, 109–144.

Stanley, S.M. and **Hardie, L.A.** (1998) Secular oscillations in the carbonate mineralogy of reef-building and sediment-producing organisms driven by tectonically forced shifts in seawater chemistry. *Palaeogeogr. Palaeoclimatol. Palaeoecol.*, **144**, 3–19.

Stevens, T., **Jestico, M.J.**, **Evans, G.** and **Kirkham, A.** (2014) Eustatic control of late Quaternary sea level change in the Arabian/Persian Gulf. *Quatern. Res.*, **82**, 175–184.

Strasser, A. (2015) Hiatuses and condensation: an estimation of time lost on a shallow carbonate platform. *Deposit. Rec.*, **1**, 91–117.

Strasser, A. and **Strohmenger, C.** (1997) Early diagenesis in Pleistocene coral reefs, southern Sinai, Egypt: response to tectonics, sea level and climate. *Sedimentology*, **44**, 537–558.

Strasser, A., **Davaud, E.** and **Jedoui, Y.** (1989) Carbonate cements in Holocene beachrock: example from Bahiret el Biban, southeastern Tunisia. *Sed. Geol.*, **62**, 89–100.

Stuiver, M. and **Reimer, P.J.** (1993) Extended 14C database and revised CALIB radiocarbon calibration program. *Radiocarbon*, **35**, 215–230.

Sugden, W. (1963) Some aspects of sedimentation in the Persian Gulf. *J. Sed. Res.*, **33**, 355–364.

Swart, P.K. (2015) The geochemistry of carbonate diagenesis: the past, present and future. *Sedimentology*, **62**, 1233–1304.

Taylor, J.C.M. and **Illing, L.V.** (1969) Holocene intertidal calcium carbonate cementation, Qatar, Persian Gulf. *Sedimentology*, **12**, 69–107.

Tribble, G.W. (1993) Organic matter oxidation and aragonite diagenesis in a coral reef. *J. Sed. Petrol.*, **63**, 523–527.

Vousdoukas, M.I., **Velegrakis, A.F.** and **Plomaritis, T.A.** (2007) Beachrock occurrence, characteristics, formation mechanisms and impacts. *Earth-Sci. Rev.*, **85**, 23–46.

Wall, M. and **Nehrke, G.** (2012) Reconstructing skeletal fiber arrangement and growth mode in the coral Porites lutea (Cnidaria, Scleractina): a confocal Raman microscopy study. *Biogeosciences*, **9**, 4885–4895.

Whitehouse, P.L. and **Bradley, S.L.** (2013) Eustatic sea level changes since the last glacial maximum. In: *Encyclopaedia of Quaternary Science*, 2nd edn (Ed. Elias, S.A.), pp. 439–451. Elsevier, Amsterdam.

Whittle, G.L., **Kendall, C.**, **St, C.**, **Dill, R.F.** and **Rouch, L.** (1993) Carbonate cement fabrics displayed: a traverse across the margin of the Bahamas Platform near Lee Stocking Island in the Exuma Cays. *Mar. Geol.*, **110**, 213–243.

Wignall, P. and **Newton, R.** (1998) Pyrite framboid diameter as a measure of oxygen deficiency in ancient mudrocks. *Am. J. Sci.*, **298**, 537–552.

Wilkin, R.T. and **Barnes, H.L.** (1997) Formation process of framboidal pyrite. *Geochim. Cosmochim. Acta*, **61**, 323–339.

Wilkinson, B.H., **Smith, A.L.** and **Lohmann, K.C.** (1985) Sparry calcite marine cement in Upper Jurassic limestones of southeastern Wyoming. In: *Carbonate Cements* (Eds Schneidermann, N. and Harris, P.M.). The society of Economic Paleontologists and Mineralogists, Special Publication, 185–220.

Zhang, T.H. and **Liu, X.Y.** (2009) Nucleation: what happens at the initial stage? *Angew. Chem. Int. Ed.*, **48**, 1308–1312.